Chromatin state transitions in the Drosophila intestinal lineage identify principles of cell-type specification

Manon Josserand, Natalia Rubanova, Marine Stefanutti, Spyridon Roumeliotis, Marion Espenel, Owen J Marshall, Nicolas Servant, Louis Gervais, Allison J Bardin

Resource

Developmental Cell

Chromatin state transitions in the *Drosophila* intestinal lineage identify principles of cell-type specification

Graphical abstract

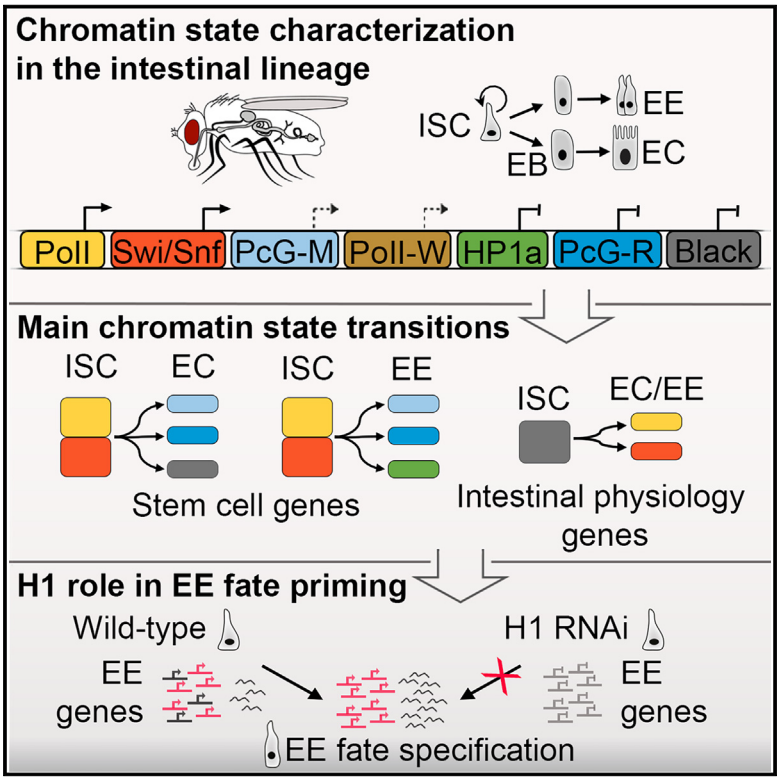

Highlights

- Genome-wide chromatin state changes occur upon intestinal stem cell differentiation
- Stem cell genes undergo lineage-specific chromatin state transitions
- Physiology-related genes are primed in a H1-enriched chromatin state in ISCs
- Histone H1 has a role in lineage priming toward the enteroendocrine fate

Authors

Manon Josserand, Natalia Rubanova, Marine Stefanutti, ..., Nicolas Servant, Louis Gervais, Allison J. Bardin

Correspondence

louis.gervais@curie.fr (L.G.), allison.bardin@curie.fr (A.J.B.)

In brief

Josserand et al. investigate chromatin state transitions associated with adult stem cell differentiation in the *Drosophila* intestinal lineage. They demonstrate cell-type-specific and common chromatin changes at genes with key functions in tissue homeostasis and identify a role for histone H1 in lineage priming.

Josserand et al., 2023, Developmental Cell *58*, 3048–3063
December 18, 2023
https://doi.org/10.1016/j.devcel.2023.11.005

CellPress

CellPress
OPEN ACCESS

Developmental Cell

Resource

Chromatin state transitions in the *Drosophila* intestinal lineage identify principles of cell-type specification

Manon Josserand,[1] Natalia Rubanova,[1,2] Marine Stefanutti,[1] Spyridon Roumeliotis,[1] Marion Espenel,[3] Owen J. Marshall,[4] Nicolas Servant,[2] Louis Gervais,[1,*] and Allison J. Bardin[1,5,*]

[1]Institut Curie, PSL Research University, Sorbonne University, CNRS UMR 3215, INSERM U934, Genetics and Developmental Biology Department, 75248 Paris, France

[2]Institut Curie Bioinformatics Core Facility, PSL Research University, INSERM U900, MINES ParisTech, Paris 75005, France

[3]Institut Curie, PSL University, ICGex Next-Generation Sequencing Platform, 75005 Paris, France

[4]Menzies Institute for Medical Research, University of Tasmania, Hobart 7000, Australia

[5]Lead contact

*Correspondence: louis.gervais@curie.fr (L.G.), allison.bardin@curie.fr (A.J.B.)

https://doi.org/10.1016/j.devcel.2023.11.005

SUMMARY

Tissue homeostasis relies on rewiring of stem cell transcriptional programs into those of differentiated cells. Here, we investigate changes in chromatin occurring in a bipotent adult stem cells. Combining mapping of chromatin-associated factors with statistical modeling, we identify genome-wide transitions during differentiation in the adult *Drosophila* intestinal stem cell (ISC) lineage. Active, stem-cell-enriched genes transition to a repressive heterochromatin protein-1-enriched state more prominently in enteroendocrine cells (EEs) than in enterocytes (ECs), in which the histone H1-enriched Black state is preeminent. In contrast, terminal differentiation genes associated with metabolic functions follow a common path from a repressive, primed, histone H1-enriched Black state in ISCs to active chromatin states in EE and EC cells. Furthermore, we find that lineage priming has an important function in adult ISCs, and we identify histone H1 as a mediator of this process. These data define underlying principles of chromatin changes during adult multipotent stem cell differentiation.

INTRODUCTION

Growing evidence supports the importance of chromatin organization in the regulation of adult stem cell proliferation, maintenance, or differentiation.[1,2] Studies using embryonic stem cells, as well as *in vivo* models, have extensively described the roles of chromatin-associated factors in stem cells during development.[3] In addition, profiling of histone modifications and chromatin accessibility showed that distinct chromatin states are established during cell lineage differentiation acting to channel developmental potential.[4–6] However, the chromatin changes associated with stem cell differentiation during adult tissue homeostasis are not well understood.

In the last 10 years, statistical modeling of combinatorial distribution of histone marks and chromatin factors has allowed a more accurate description of the landscapes of epigenetic complexity in various genomes, including those of humans and flies.[7–11] In *Drosophila* cell lines, a model of five main chromatin types was established based on the binding combinations of 53 chromatin-associated proteins.[8] Such modeling has enabled the characterization of chromatin changes during development by integrating genome-wide maps of chromatin features across developmental stages in various tissues.[11–14] Studies in mammalian adult tissues, such as the skin, hematopoietic system, and the intestine, highlighted changes at enhancers during cell-type specification by profiling a limited set of chromatin marks, including histone H3 methylation and acetylation (H3K27me3, H3K4me, and H3K27ac), as well as chromatin accessibility.[15–21] However, broader combinatorial modeling of chromatin state changes has not been described in adult stem cell lineages.

Drosophila adult midgut intestinal stem cells (ISCs) possess a low basal rate of self-renewal, which can be enhanced upon injury response and cues from the environment.[22–25] ISCs give rise to intermediate progenitors, enteroblasts (EBs), and enteroendocrine precursors (EEPs), which differentiate into enterocytes (ECs) and enteroendocrine cells (EEs), respectively (Figure 1A).[24–26] Although the *Drosophila* intestinal lineage has been used to study the regulation of stem cell proliferation and cell-fate specification by transcription factors (TFs),[27] less is known about the chromatin organization in ISCs and their progeny. We and others have provided evidence for chromatin factors controlling ISC proliferation and differentiation, highlighting their importance in the regulation of the lineage.[28–37]

CellPress
OPEN ACCESS

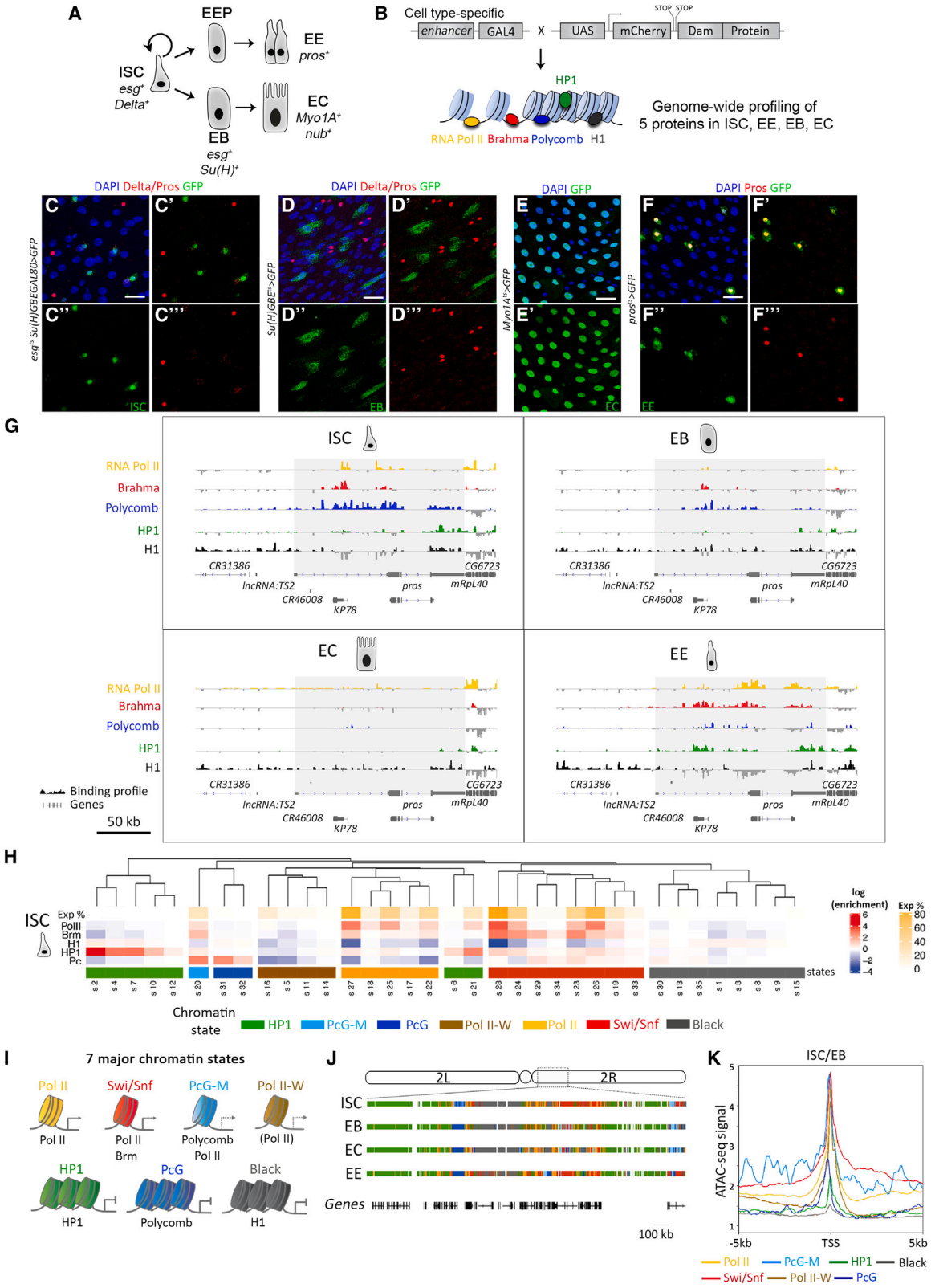

Figure 1. Chromatin state modeling identifies seven major chromatin states in the midgut

(A) Intestinal lineage cells and markers.

(B) Experimental setup of targeted DamID.

(legend continued on next page)

Notwithstanding these studies, an understanding of chromatin organization in the lineage at the genome-wide scale is lacking.

The role of the linker histone H1 in stem cells and, in particular, in adult stem cells, has been less studied than core-histones and their modifications, despite a function in the modulation of nucleosome and chromatin architecture.[38–40] This is in part due to the redundancy of variants of linker histone H1 in mammals. With only one somatic variant of H1,[41] *Drosophila* is a useful model to address its function in adult stem cells. To date, H1 is known to be required in germline stem cells of the *Drosophila* ovary to prevent their differentiation through activation of differentiation factor *bam*,[42] but its role in adult somatic stem cells in a homeostatic tissue has not been investigated.

Here, we use the *Drosophila* midgut to investigate lineage-specific changes in chromatin states upon adult stem cell differentiation. We identify chromatin state transitions associated with stem cell differentiation during tissue homeostasis by cell-type-specific profiling of chromatin proteins and subsequent cell-type-specific chromatin state modeling, providing a large resource for the scientific community. We find that the histone H1-enriched Black state is involved in major chromatin state transitions affecting both stem cell and lineage-specific genes. Our data further suggest a role for H1 in lineage priming toward the EE fate. These findings identify principles of cell-type specification in an adult tissue.

RESULTS

Cell-type-specific modeling of chromatin states in ISCs and their progeny

To characterize chromatin states in adult ISCs and their progeny, we took advantage of targeted DNA adenine methyltransferase identification (DamID),[43,44] previously used to identify chromatin states in the neuroblast lineage of the developing *Drosophila* brain.[11] DamID relies on the tethering of the Dam methyltransferase from *E. coli* to a protein of interest, allowing methylation of adenine on GATC DNA sequences surrounding the binding sites of the protein of interest. Methylated GATC sites can thereby be detected via enzymatic digestion and whole-genome sequencing.[45] We profiled in a cell-type-specific manner the distribution of five chromatin-associated proteins from which the previously described five major types of chromatin can be inferred[8,11]: the core subunit of RNA polymerase II (RNA Pol II) and Brahma (Brm, a Swi/Snf complex member) for active chromatin states, Polycomb (Pc), heterochromatin protein 1a (hereafter referred to as HP1), and histone H1 for repressive chromatin states. Whole-genome binding maps were generated in EBs, EEs, and ECs (Figure 1B), and we used our previously generated ISC-profiling datasets of these factors.[32] Cell-type specificity of the GAL4 drivers was verified by combining GFP expression and immunostaining of specific markers of ISCs (Delta), and EEs (Pros), and the nuclear size of polyploid ECs (nucleus diameter > 7 μm). EBs are diploid (nucleus diameter < 7 μm) and negative for Delta and Pros (Figures 1C–1F‴). The EEPs could not be profiled as an efficient, specific GAL4 driver is not available. Dam construct expression specificity was also validated (Figures S1A–S1D′). The binding profiles of the five proteins in all cell types were predictably associated with known genomic loci and features, such as HP1 at pericentromeric heterochromatin and Pc along *Hox* clusters (Figures S2A–S2C). The chromatin environment of genes known to be expressed in a cell-type-specific manner in the lineage (Figures 1G, S2D, and S2E) were consistent with expectations.

Next, we defined genome-wide chromatin states by using hidden Markov modeling (HMM), probabilistic modeling that captures the diversity of the observed protein binding combinations obtained by targeted DamID, as well as their spatial genomic distribution relative to each other (or transition probabilities; Figures 1H and S3A). For each cell type, a 35-state model was fit. Modeling was followed by further clustering into seven major groups (Figures 1H and S3A). These seven groups separated into distinct regions in principal-component analysis (PCA) space (Figure S3B). The distinct chromatin states were named for their primary enriched protein (Figure 1I). Genome-wide maps of chromatin states were generated (Figures 1J, S3C, and S3D). We identified two active states (RNA Pol II or "Pol II" state and "Swi/Snf" state) similar to the Yellow and Red/Swi/Snf previously described.[8,11,46] The Pol II state was enriched in RNA Pol II with some Brm and HP1, whereas it was depleted for Pc and H1. The Swi/Snf state was enriched in Brm with some HP1 and Pc binding. Furthermore, the model detected the three repressive states defined previously,[8] here named the "Polycomb group" (PcG) and "HP1" states, enriched in Pc and HP1, respectively, as well as the "Black"/null state devoid of all factors binding with the exception of some H1 enrichment. Our model also detected two "intermediate" states, displaying features of both active and repressive chromatin. First, there was another Pc-enriched state also defined by RNA Pol II and Brm binding, hence named "PcG-mixed" (PcG-M). A similar signature was described in the developing brain.[11] Second, a RNA Pol II weak (RNA Pol II-W) state was found, similar to the Pol II state but with a lower RNA Pol II occupancy (Figures 1H and S3A).

(C–F‴) Representative images of midguts expressing GFP (green) in ISCs under the control of *esg*^{ts} *Su(H)GBE-GAL80* driver (C); in EBs with the *Su(H)GBE*^{ts} (D); in ECs under the control of *Myo*^{ts} driver (E); in EEs under the control of *pros*^{ts} (F). Nuclei stained with DAPI are in blue, and Delta and Pros are in red. Scale bars, 20 μm.

(G) DamID binding profiles of RNA Pol II, Brahma, Polycomb, HP1, and H1 in the four cell types at EE marker gene locus, *pros*.

(H) HMM-fitted 35-state model for ISCs. Each column is a state, named as a number (bottom). The first line (yellow color scale) represents the proportion of expressed genes (Exp %) in each state determined by RNA Pol II mean occupancy along gene bodies. The five next lines (blue to red scale, log[enrichment]) represent the mean binding intensity of proteins in each state. Dendrogram shows state clustering based on state-state transition probabilities. The colored bars at the bottom represent the clustering of states into groups (HP1, PcG-M, PcG, Pol II-W, Pol II, Swi/Snf, and Black) kept for further analyses.

(I) Schematic representing the seven major chromatin states interpreted as active (Pol II and Swi/Snf), intermediate (PcG-M and Pol II-W), and repressive (HP1, PcG, and Black). Proteins enriched in each state are indicated.

(J) Chromatin state maps in the four cell types on a portion of chromosome 2R, near the centromere.

(K) Chromatin accessibility levels as defined by ATAC-seq on FACS-sorted ISCs/EBs at the TSS of genes grouped by chromatin state. Each curve shows the mean ATAC-seq signal value around the transcription start sites (TSS) (±5 kb) of the genes classified by their chromatin state.

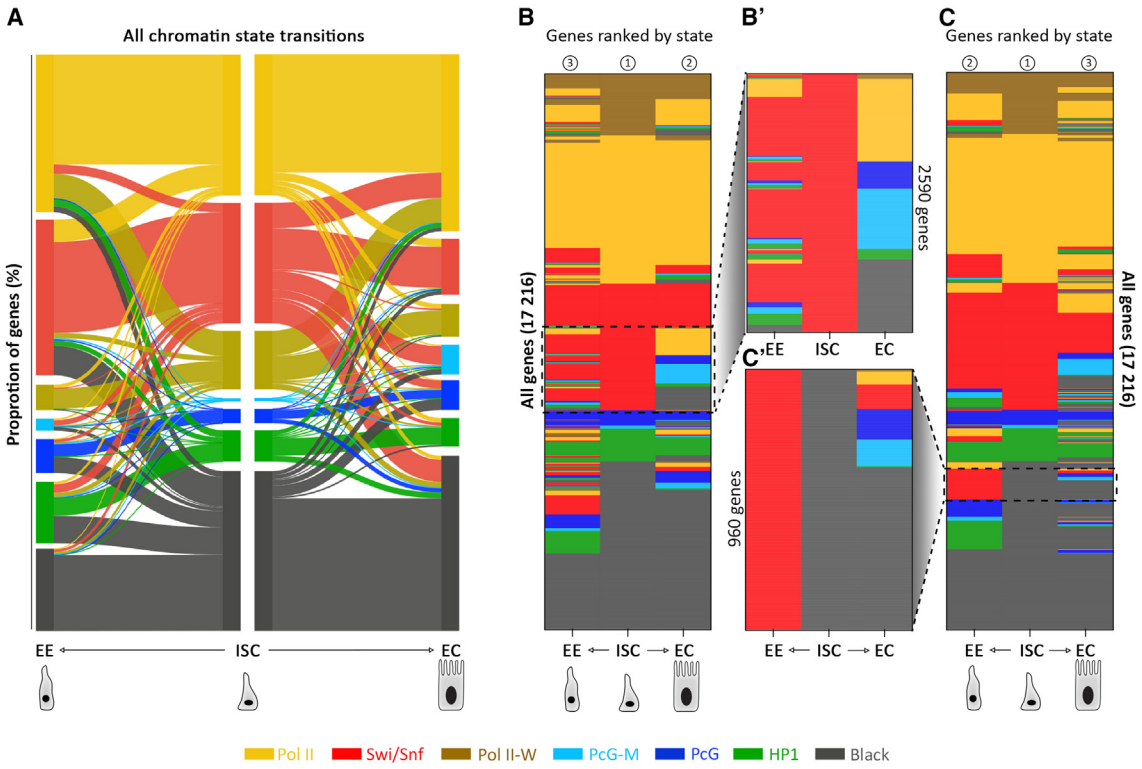

Figure 2. Lineage-specific chromatin state transitions at genes upon ISC differentiation

(A) Chromatin state transitions between ISCs and ECs, ISCs and EEs. Boxes represent the proportion of genes marked by each chromatin state. The flows represent the proportion of genes undergoing chromatin state transitions from one state to another between cell types.

(B and C) Colored maps of genes in chromatin states in ISCs, ECs, and EEs. Each row is a gene with its corresponding chromatin state in each cell type. Genes are ranked by chromatin state, in the order indicated by the numbers above the map. (B′) and (C′) are enlarged zooms of the framed regions in (B) and (C), respectively.

We then assessed the relationship between chromatin states, gene expression, and chromatin accessibility. To this aim, we combined chromatin accessibility profiling using targeted DamID (CATaDa) for each cell type (Figure S3E),[47] an assay for transposase-accessible chromatin followed by sequencing (ATAC-seq) on fluorescence-activated cell sorting (FACS)-sorted ISCs/EBs (Figure 1K), and available cell-type-specific RNA sequencing (RNA-seq) (Figure S3F).[48] Pol II and Swi/Snf states displayed the highest values of transcript levels and chromatin accessibility, whereas HP1, PcG, and Black states had the lowest (Figures 1K, S3E, and S3F). Genes marked by the Pol II-W state displayed lower average transcript levels than genes marked by the Pol II state (Figure S3F). The PcG-M state showed accessibility levels comparable to the ones in Pol II or Swi/Snf states despite an enrichment in Pc binding but lower average transcript levels (Figures 1K, S3E, and S3F). This suggests that genes marked by this state may either be in a permissive, poised, or heterogeneous state within the cell population. Therefore, comparing chromatin states with chromatin accessibility and transcript levels validated our categorization of active, intermediate, and repressive states.

Overall, our genome-wide characterization of chromatin states in the intestinal lineage highlighted the general features of the distinct chromatin types that are conserved among midgut cell types.

Lineage-specific chromatin state transitions of genes during differentiation

We then assessed the chromatin changes that underlie adult stem cell differentiation in the intestinal lineage. Comparing the genomic coverage of the seven chromatin states between cell types (ISC vs. EB, EB vs. EC, and ISC vs. EE) identified genome-wide transitions during the differentiation process (Figure S4). We hypothesized that distinct chromatin state transitions may mark different classes of genes undergoing transcription changes during differentiation. To assess this, a single chromatin state was assigned to each gene based on the predominant state covering the entire gene.

We then determined the distribution of all genes in chromatin states in the different intestinal cell types. 60% of genes underwent at least one chromatin state change upon ISC differentiation, highlighting the extent of chromatin remodeling throughout the differentiation process (Figures 2A and 2B; Table S1). Interestingly, differences were apparent between EE and EC lineages in the main chromatin state transitions. The proportion of genes in the active Swi/Snf state in ISCs was reduced upon EC differentiation yet expanded upon EE differentiation, whereas the proportion of genes in the Pol II state was not greatly altered (Figures 2A and 2B). 67% of the genes that exited the Swi/Snf state from ISCs to ECs, remained in the Swi/Snf state in EEs (Figure 2B′). This indicates that active chromatin states of genes are

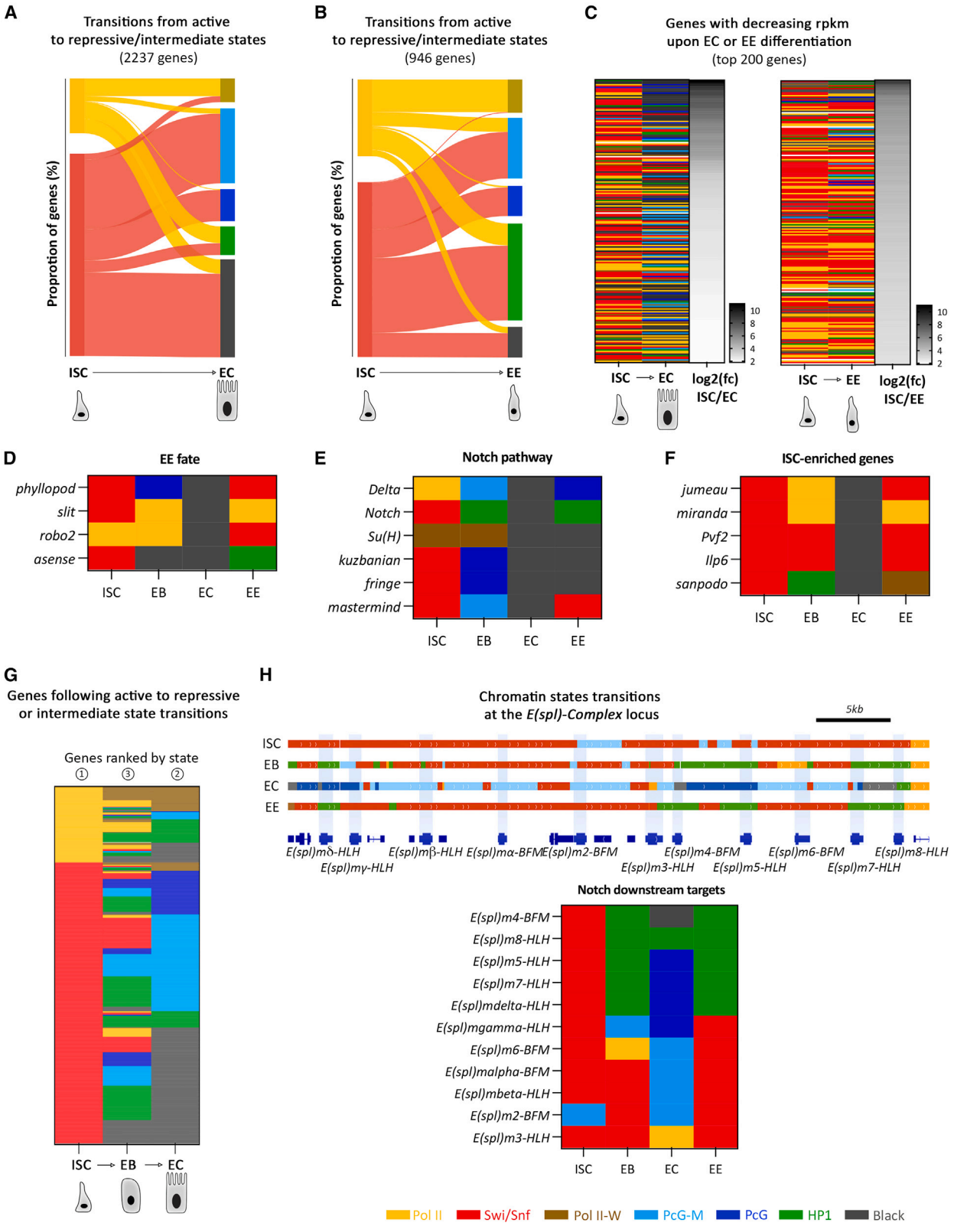

(legend on next page)

more conserved during ISC to EE differentiation than during ISC to EC differentiation. Furthermore, a large proportion of genes in the repressive Black state in ISCs acquired the Swi/Snf state during differentiation to EEs while remaining in the Black state in ECs (Figures 2C and 2C′). Thus, although EEs share more genes with ISCs in active states, ECs have more genes in common with ISCs in repressive states.

Stem cell differentiation is associated with silencing of transcriptional programs conferring stem cell properties. HP1-associated chromatin has been proposed to expand in the genome of differentiated cells and to serve as a lock repressing stem cell genes during development.[11,49–53] We therefore investigated how stem cell genes are turned off during differentiation by focusing on genes switching from active chromatin states (Pol II/Swi/Snf) in ISCs to intermediate or repressive states in ECs or EEs (Figures 3A and 3B). EC differentiation was associated with a high proportion of genes transitioning from active states to the H1-enriched Black state (Figure 3A), whereas EE differentiation was instead characterized by a high proportion of genes transitioning to the HP1 state (Figure 3B). Interestingly, key regulators of ISC differentiation such as *Notch* and *asense* followed this lineage-specific transitions because they were found in the Black state in ECs and in the HP1 state in EEs (Figures 3D and 3E; Table S1). This suggests that the lock for repression of stem cell genes in differentiated cells previously associated with HP1 chromatin might also apply to the Black chromatin state in ECs.

We also found that many genes followed a transition from active states to the Pc-enriched PcG-M and PcG states, in similar proportions between ECs and EEs (Figures 3A and 3B). These data suggest that different repressive chromatin states may be employed to regulate gene expression during differentiation. Furthermore, we noticed that genes whose transcript levels decrease upon EC or EE differentiation (top 200 genes by decreasing $\log_2$fold-change [FC]) were found predominantly in the repressive PcG and Black states in ECs, whereas in EEs most of these genes remained in active chromatin states (Figure 3C). This was notably observed for ISC-enriched genes with reduced transcript levels in ECs and EEs[48] and found in the Black state in ECs but still in active states in EEs (Figure 3F). This suggests that a decrease in the expression of these genes in EEs is not always associated with a repressive chromatin state.

To better understand the differentiation process of the EC lineage, we further explored the "active to repressive" chromatin state changes from ISCs to EBs, the precursors of ECs (Figure 1A). Our data identified several major intermediate transitions with genes in Swi/Snf active states in ISCs, passing through diverse chromatin states in EBs, prior to acquiring repressive states in ECs (Figure 3G). These included genes important for EE lineage specification, such as *phyl*, *slit*, *robo2*, and *ase* (Figure 3D), and genes playing a role in EC differentiation, such as components of the *Notch* signaling pathway and *Notch* downstream targets (Figures 3E and 3H). These data suggest that, during the differentiation process, sequential steps of chromatin remodeling occur, exchanging repressive states. Altogether, these data suggest that genes undergo major chromatin state changes that are distinct upon differentiation to the EC or EE lineage.

Regulation of stem cell and lineage TFs involves the Pc-enriched PcG-M and PcG-repressive states

Because lineage decisions are driven by expression of key TFs, we assessed the chromatin states of TF-encoding genes using a list of 885 annotated TFs from the Gene List Annotation for Drosophila (GLAD) database.[54] TF-encoding genes were significantly enriched in the Pc-associated PcG state compared with the distribution of all genes in chromatin states in all cell types (Figure 4A). Focusing on the TFs that underwent chromatin changes during differentiation, the main TFs known for their role in the regulation of ISCs (*esg*, *wor*, *Sox100B*, *Ets21c*, and *klu*) were found in active states in ISCs and/or EBs and were marked by the PcG or PcG-M state in ECs (Figure 4B). This trend was also found with genes of the *E(spl)-Complex* (Figure 3H). Similarly, in EEs, *esg*, *wor*, and *klu* were found in a repressive PcG state, whereas *Sox100B* and *Ets21c* were instead in a Swi/Snf state (Figure 4B).

Our data further suggest that Pc-enriched chromatin states mark TFs important for the regulation of the intestinal lineage, which are turned on or off upon differentiation. Indeed, the primary TFs controlling differentiation were marked by the PcG state in ISCs and transitioned to active Swi/Snf or Pol II states during EE or EC differentiation (Figure 4C). These include *nubbin* (*pdm1*), important for EC specification, and *prospero*, *mirror*, and *Pox neuro*, important within the EE lineage (Figure 4C). To further test the functional relevance of Pc-mediated silencing in ISCs for repression of lineage TF genes, we compared chromatin states in ISCs with the differentially accessible regions and deregulated genes in *Pc* knockdown context using published data[35] (Figures S5A–S5C). Although only minor changes in chromatin accessibility occurred upon *Pc* knockdown, regions that gained accessibility or increase RNA expression in *Pc* RNAi were mainly in the PcG and Black states (Figures S5A and S5C), consistent with a role for Pc in maintaining a repressive chromatin state. However, *prospero*, *mirror*, *Pox neuro*, and *nubbin* did not have differentially accessible peaks and were not upregulated in *Pc*

Figure 3. Gene expression changes during differentiation correlate with various chromatin state transitions

(A and B) Chromatin state transitions from ISC active to repressive/intermediate states in ECs (A) and EEs (B).

(C) Colored map of genes following a decrease in transcript levels reads per kilobase per million (rpkm) upon EC or EE differentiation. Genes with rpkm>1 in ISCs were sorted by decreasing $\log_2$(FC) and the top 200 genes are shown.

(D and E) Chromatin states of genes with important functions in ISC differentiation toward EE (D) and EC fates (E) showing intermediate, lineage-specific transitions upon differentiation.

(F) Chromatin states of genes enriched in ISCs.

(G) Colored map of genes following the "active to repressive/intermediate state" transitions, from ISCs to ECs. Genes are sorted by chromatin state, in the order indicated by the numbers above the map.

(H) Chromatin states of Notch downstream target genes at the *E(spl)-Complex* locus in ISCs, EBs, ECs, and EEs showing intermediate, lineage-specific transitions upon differentiation.

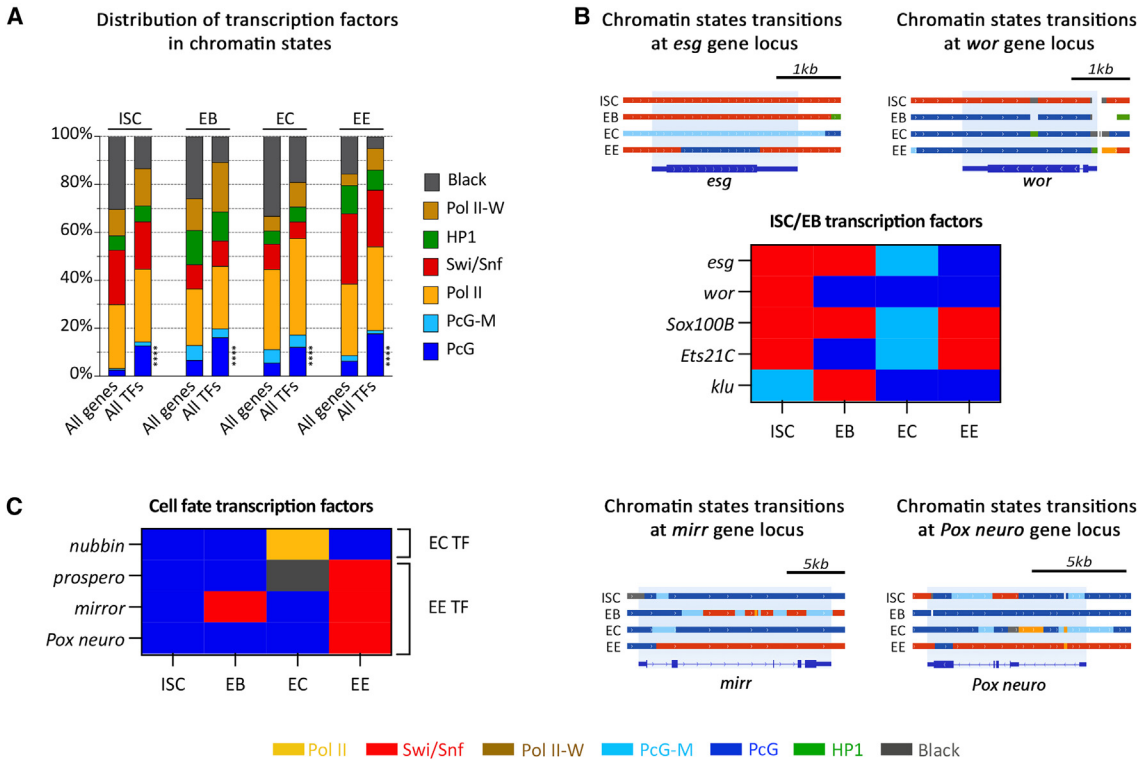

Figure 4. Regulation of stem cell and lineage transcription factors involves the Polycomb-enriched PcG and PcG-M chromatin states

(A) Distribution of 885 genes encoding transcription factors in chromatin states in each cell type, compared with the distribution of all genes. Transcription factors are significantly enriched in the PcG state compared with all genes (****$p < 0.0001$ for the 4 cell types, Fisher's exact test).

(B and C) Chromatin states of subsets of TF-encoding genes with important functions in ISC regulation (B) or in cell-fate specification (C).

knockdown context, suggesting that Pc binding at these genes is a mark of their repressive state but is not required for their repression. It is likely that redundant mechanisms ensure the repression of these important lineage regulators.

Physiology-related genes are marked by the Black state in ISCs

To gain insight into the chromatin state transitions during the differentiation process, we examined the genes marked by the inactive states (Black, HP1, and PcG) in ISCs and found in the active states (Pol II and Swi/Snf) in EEs and ECs (Figures 5A and 5D). Although there was no significant enrichment in gene ontology (GO) terms for the genes following a "HP1 to active" or a "PcG to active" transitions, a significant enrichment in GO categories related to the EE-specific functions such as ion transport, neuropeptide secretion, and signaling for the genes following a "Black to active" transition upon EE differentiation was found (Figure 5B). Consistent with this, a set of 321 EE-enriched genes (Table S2) with functions related to EE physiology showed that the "Black to Swi/Snf" chromatin state transition was predominant upon ISC to EE differentiation (Figure 5C).

We then tested the hypothesis that genes following a Black to active transition upon EC differentiation would be similarly enriched for EC-specific physiology-related functions. First, GO analysis resulted in significant enrichment of "proteolysis," "long-chain fatty acid metabolic process," and terms related to digestive enzymatic activity (Figure 5E). Second, 226 genes encoding midgut-enriched digestive enzymes[55] were assessed for chromatin state changes, and, indeed, among the genes that changed states, a major transition type was Black to Swi/Snf (Figure 5F). In addition, many of the digestive enzyme-encoding genes were found already to be expressed at high levels in ISCs in RNA-seq data[48] and remained in Swi/Snf or Pol II states throughout differentiation (Figure 5F; Table S3). Together, these results show that during the differentiation process, a transition from a repressive Black state to an active state is the major chromatin state transition of genes encoding metabolic enzymes and physiological functions of differentiated cells. In line with these data, the genes undergoing the Black to active transition upon EE or EC differentiation have increasing transcript levels during differentiation[48] (Figures 5G and 5H).

We compared the chromatin accessibility at the TSS of these genes switching from Black to active chromatin vs. genes that remain in a Black state using our ATAC-seq data from ISCs/EBs. Three classes were defined: (1) genes in a Black state in all cell types ("Black stable"), (2) genes transitioning from Black to active upon EE differentiation, and (3) genes transitioning from Black to active in ECs (Figure 5I). The TSSs of genes that acquire active states in differentiated cells (classes 2 and 3) were more accessible than the genes of the Black stable class. In addition, despite low transcript levels (mean transcripts per million [tpm] < 2) in ISCs for genes of the three classes, genes from classes 2 and 3 displayed on average higher transcript levels than genes from the Black stable class (Figure 5J). This suggests

CellPress
OPEN ACCESS

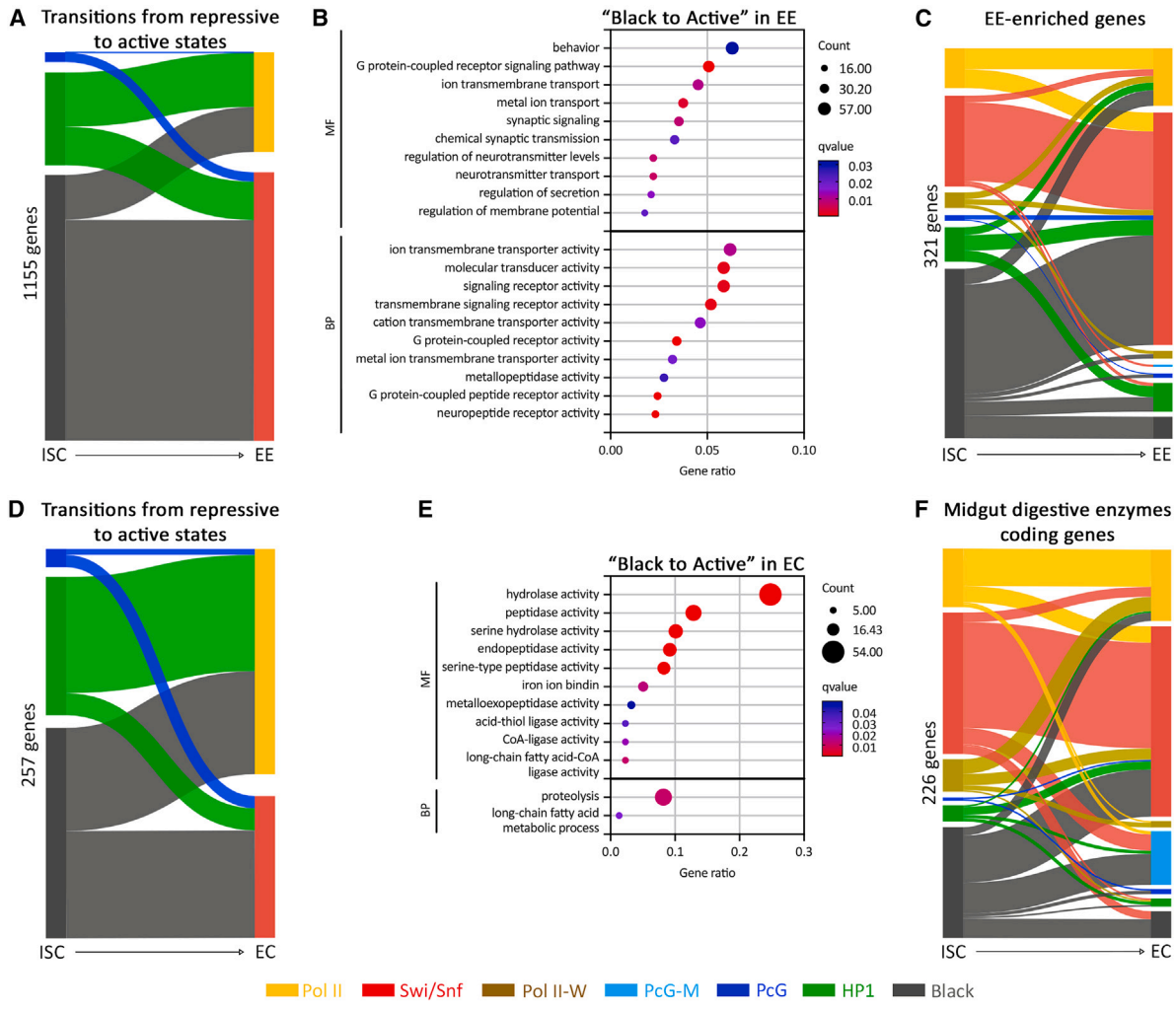

Figure 5. Physiology-related genes undergo a Black to active transition upon their activation

(A) Chromatin state transitions of genes marked by a repressive state in ISCs and an active state in EEs.

(B) GO terms enriched in the genes undergoing the Black to active transition in EEs. MF, molecular function; BP, biological process.

(legend continued on next page)

that, in ISCs, the transcriptional program of differentiated cells is primed for activation. Thus, although these genes are all in the Black chromatin state in ISCs as defined in our model, additional regulation likely acts to tune the chromatin accessibility required for future transcription of these genes upon differentiation.

Histone H1 is required for correct expression of EE-identity genes in ISCs

Our data above showed that H1 protein binding was enriched in the Black state, which is associated with chromatin changes at genes with key functions in cell fate and intestinal physiology. H1 binding was also found in the HP1 state, consistent with its known functions in heterochromatin establishment.[56,57] Histone H1 has been shown to be important for nucleosome compaction and heterochromatin formation in *Drosophila* embryonic tissues[56–58] and in the hematopoietic system.[59] Therefore, to understand the functional role of histone H1, we investigated the effects on chromatin accessibility and gene expression of *H1* knockdown in ISCs and EBs.

To this aim, we performed ATAC-seq and RNA-seq on FACS-sorted ISCs and EBs from intestines expressing RNAi against *H1* in ISCs/EBs for 4 days, using the *esg-GAL4* driver combined with a *tubulin-GAL80^{ts}* ("*esg^{ts}*"; Figure 6A). Among deregulated genes in ISCs/EBs upon *H1* knockdown (Figure 6B; Table S4), the most upregulated genes (24/35 genes with a $\log_2$FC > 2) were found in the repressive Black or HP1 states in ISCs/EBs (Figure 6C) and had low transcript levels in all cell types (published RNA-seq data[48]) (Table S4). This is consistent with a role of H1 in maintaining the repression of these genes in the intestine. Nevertheless, a majority of the upregulated genes were in the Swi/Snf, Pol II, or Pol II-W states in ISCs/EBs (Figures 6C and 6D) that lack H1 binding, suggesting an indirect or longer-range effect of *H1* knockdown on their expression.

Surprisingly, GO analysis on downregulated genes showed an enrichment for neuropeptide secretion and signaling functions, characteristic of the EE transcriptional program and metabolic function (Figure 6E). Indeed, 68% of the downregulated genes in ISCs/EBs upon *H1* knockdown show increased expression upon ISC to EE lineage differentiation,[48] and 31% of these genes are associated with a chromatin state transition from Black in ISCs to Pol II/Swi/Snf in EEs (Figure 6F). Comparing downregulated genes in *H1* knockdown with a list of EE-enriched genes further demonstrated an enrichment in EE genes, including TFs involved in EE fate such as *prospero* and *mirror* (Figure 6G; Table S4). This was not due to changes in ISC/EB cell proportions (Figures S6A–S6I). Therefore, despite low expression of EE-identity associated genes in ISCs/EBs, *H1* knockdown caused a global downregulation of these genes in ISCs/EBs.

The knockdown of H1 caused relatively few changes to chromatin accessibility in the population of ISCs and EBs (Figure 6H; Table S5). Although RNAi depletion of H1 resulted in only a partial loss of the protein (Figures S6A–S6E), differentially accessible peaks were nevertheless widely distributed along the genome (Figure 6I). Increased ATAC-seq peaks were found predominantly in the HP1 and Black states, whereas decreased peaks were located mostly in the Swi/Snf state in ISCs (Figure 6J). Consistent with a change in EE-identity gene expression upon *H1* knockdown, motif enrichment analysis on less accessible peaks showed enrichment for the predicted binding sites of Scute (Sc) and Asense (Ase), important EE fate TFs (Figure 6K). Together these data point toward a role of H1 in EE gene priming in progenitor cells through the maintenance of chromatin accessibility for EE fate TFs.

Histone H1 is required for ISC-lineage priming toward the EE fate

We next asked whether H1 activity in ISCs/EBs may be important to promote EE differentiation. *H1* RNAi was expressed in ISCs/EBs for 4 and 21 days using *esg^{ts}* (Figures 7A–7J). We used three *H1* RNAi lines, which all showed a significant decrease in H1 signal intensity in *esg^{+}* cells after 4 days of expression (Figures S6A–S6E). The proportions of EEs were significantly reduced in midguts expressing *H1* RNAi in ISCs/EBs for 21 days (three *H1* RNAi lines, Figures 7D–7J), although not at 4 days (Figures 7A–7C), a time point at which EEs would not yet have undergone turnover. Thus, H1 in progenitor cells promotes the production of new EEs. Consistent with this, lineage tracing using the flp-out system from stem cells demonstrated that *H1* knockdown significantly reduced EE proportion (two out of three RNAi lines having the most H1 depletion; Figures S7A–S7H). In contrast, EC differentiation was not affected (Figure S7D). This indicates that H1 is required in the lineage for the correct production of EEs. To determine the cell type in which H1 activity is required to regulate EE fate, we induced *H1* knockdown in a cell-type-specific manner (Figures S7I–S7Q). A reduction in EE numbers was observed when *H1* RNAi was expressed only in ISCs (Figures S7I–S7K) but not when expressed specifically in EBs (Figures S7L–S7N) or EEs (Figures S7O–S7Q), demonstrating that H1 is required in ISCs for future EE differentiation. Taken together, these results indicate that H1 has a function in EE lineage priming; it is required to promote basal levels of expression of EE-identity genes in ISCs and for their differentiation toward EE fate.

DISCUSSION

In this study, we investigated the chromatin state transitions occurring during differentiation in the *Drosophila* intestinal lineage. By generating cell-type-specific chromatin state maps, we highlighted differences in the major chromatin state changes

(C) Chromatin state transitions of EE-enriched genes (see STAR Methods) upon EE differentiation.
(D) Chromatin state transitions of genes marked by a repressive state in ISCs and an active state in ECs.
(E) GO terms enriched in the genes undergoing the Black to active transition in ECs.
(F) Chromatin state transitions of genes encoding midgut digestive enzymes upon EC differentiation.
(G and H) Transcript levels of genes undergoing the Black to active transition in EEs (G) and in ECs (H).
(I) Chromatin accessibility levels as defined by ATAC-seq in ISCs/EBs at the TSS of genes remaining in the Black state (Black stable) in the lineage or undergoing the Black to active transition upon differentiation toward EC or EE.
(J) ISC transcript levels of genes categorized as Black stable or Black to active upon differentiation. (G, H, and J) Match-paired Wilcoxon statistical test, mean values in red, error bars are SEM, ****$p < 0.0001$.

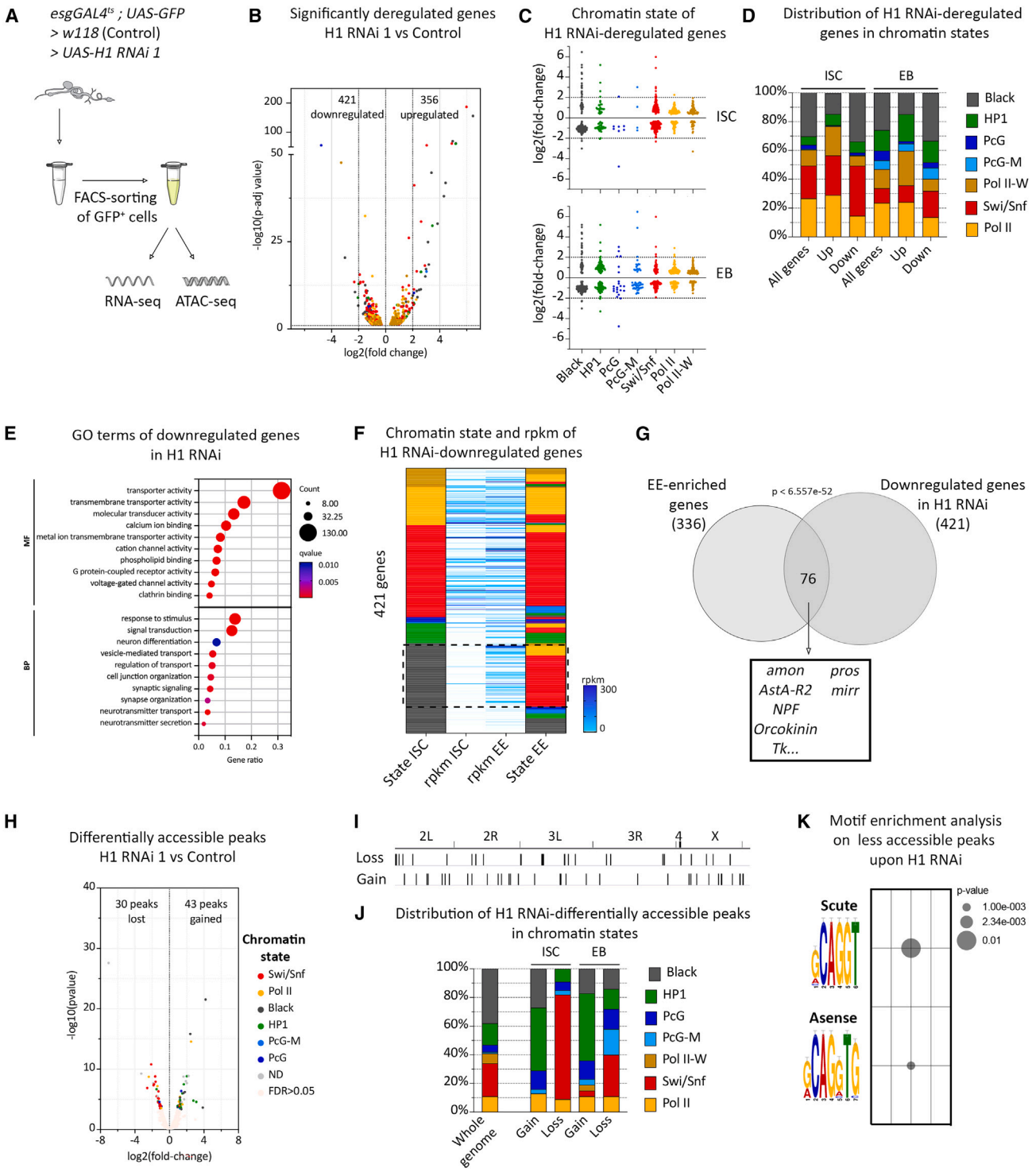

Figure 6. *H1* knockdown alters the transcription of EE-identity genes

(A) Experimental setup for RNA-seq and ATAC-seq on isolated ISCs/EBs.

(B) Volcano plot of deregulated genes upon *H1* knockdown in ISCs/EBs. Dot color represents the chromatin state of the corresponding gene in ISCs.

(C) Chromatin states of deregulated genes in ISCs and EBs.

(D) Chromatin state distribution of upregulated and downregulated genes compared with the chromatin states distribution of all genes in ISCs and EBs.

(E) GO terms enriched in genes downregulated upon *H1* knockdown.

(F) Chromatin state and transcript levels in ISCs and EEs of genes downregulated upon *H1* knockdown. The framed region highlights genes undergoing the Black to active transition with a transcription increase upon ISC to EE differentiation.

(legend continued on next page)

followed by functionally distinct groups of genes such as stem cell-associated genes, cell-fate regulators, and physiology-related genes. Our further chromatin accessibility and functional analyses suggest that lineage priming has a key function in adult ISCs and show that histone H1 promotes this process.

Modeling chromatin states in a tissue with two alternative differentiation paths indicated that distinct chromatin remodeling events accompany commitment toward the EE and EC lineages. Interestingly, 67% of genes that have enriched expression in ISCs (''stem cell genes'') but downregulated at the transcriptional level in EEs, are still marked by a Swi/Snf state, unchanged from their initial state in ISCs. This suggests that their transcriptional status in EEs might rely on the recruitment of transcriptional activators or repressors to permissive chromatin. This differs markedly from the situation in ECs, where a proportion of stem cell genes are found in repressive chromatin states, in particular in the Black state, which accompany transcriptional downregulation. Why stem-cell-enriched genes are regulated in different ways upon EE or EC differentiation remains an open question, although it could allow plasticity of the EE fate. Indeed, in the mouse intestine, it has been shown that chromatin remains broadly permissive in stem cells and committed progenitors, allowing plasticity for TF binding at enhancers.[60]

Pc-mediated repression of differentiation genes has been extensively characterized in embryonic stem cells.[61] In *Drosophila* adult stem cells, many studies addressed the roles of various PcG components in controlling stem cell self-renewal and differentiation, as well as lineage identity, in the germline[62–68] and in the intestine.[35] Pc function has also recently become a focus of interest in adult stem cells in mammals.[69] Our data showed that TFs with important roles in the regulation of the intestinal lineage are marked by Pc-enriched PcG-M or PcG states. In this work, the PcG state marks genes encoding the cell-fate regulators of EC and EE lineages in ISCs. However, it was shown that loss of Pc in ISCs does not lead to derepression of these genes, arguing against an instructive role in maintaining repression.[35] Surprisingly, the authors found instead that several genes involved in early cell-fate decisions toward the EE fate were downregulated in *Pc* knockdown context, consistent with a decrease in the number of $Pros^{+}$ EEs in the midguts expressing *E(z)* or *Pc* RNAi in ISCs and their progeny. Here, we did not find that these genes were marked by a Pc-enriched state or bound by Pc, suggesting indirect regulation. polycomb repressive complex 2 (PRC2) was found to be dispensable for maintaining quiescent hair follicle stem cell identity despite changes in their transcriptome, arguing against an instructive role in preventing premature activation or differentiation of adult stem cells.[70] Thus, our data and other studies suggest that, despite being markers of important cell-fate regulator genes, exactly how PcG proteins affect adult stem cell lineages may be complex and remains to be further investigated.

Our chromatin state modeling approach allowed us to explore other types of chromatin in stem cells beyond the frequently profiled H3K27me3, H3K4me3, and H3K27ac marks. Importantly, our data suggest that distinct functional groups of genes are silenced in different ways. In particular, we identified the Black to active transition as the predominant type of transition associated with turning on gene expression during differentiation in EE and ECs. We found that genes marked by this transition relate to the physiological functions of differentiated cells. In the developing brain, it was also shown that genes becoming active during neuronal differentiation are initially marked by the Black state in neural stem cells.[11] Given the similarities between neurons and EEs, gene silencing in the Black state could be seen as a feature of neuronal-type genes. However, the fact that many genes involved in EC-specific metabolism were also silenced in the Black state leads us to propose it as a general signature of physiology-related genes in ISCs and possibly other adult lineages. The Black state represents a compacted chromatin without commonly profiled histone modifications; therefore, it is possible that TFs could help prime these genes, consistent with our chromatin accessibility data. In addition, nuclear lamina association had been suggested to regulate the Black state[8] and could, therefore, play a role.

Finally, our study uncovered a role for histone H1 in EE lineage priming. Although H1 is widely distributed throughout the genome, it is enriched in heterochromatin and mostly associated with repressed genes, whereas it is depleted at promoters of actively transcribed genes,[71] which we also observed in the *Drosophila* intestine. H1 is much more mobile than nucleosomal histones (H2A, H2B, H3, and H4).[72,73] H1 depletion in mammalian embryonic stem cells does not affect global transcription but rather the expression of specific genes (both upregulated and downregulated) and reduces nucleosome spacing locally.[74] Other studies in human cancer cells and mouse hematopoietic cells demonstrated that H1 depletion leads to altered chromatin accessibility, H3K27me3 decrease, H3K36me3 increase, and derepression of genes located in regions that decompact.[59,75,76] A recent study also reported alteration of topologically associated domains (TADs) upon *H1* knockdown, associated to local gene deregulation.[77] Thus, beyond H1 roles in chromatin compaction in heterochromatin, it is likely that H1 also influences transcription locally in more specific ways. Our RNA-seq analysis indicated that H1 is required for the basal expression of a subset of genes that are characteristic of the EE transcriptional program. Many of these genes follow the Black to active transition previously identified. We further showed that H1 is required in ISCs to properly renew EEs in the midgut. Thus, we propose that H1 has a role in priming ISCs toward the EE fate, likely facilitating their future activation upon differentiation. Further investigation will show how H1 could mediate this function. We hypothesize that H1 could either maintain a chromatin structure promoting low or stochastic transcription at these EE-identity

(G) Overlap between genes downregulated upon *H1* knockdown and a list of EE-enriched genes (see STAR Methods), with examples of EE markers. Significance assessed with a hypergeometric test.
(H) Volcano plot of more (gain) or less (loss) accessible peaks upon *H1* knockdown.
(I) Genomic distribution of differentially accessible peaks upon *H1* knockdown.
(J) Chromatin states of the differentially accessible peaks upon *H1* knockdown, compared with the chromatin state distribution along the whole genome.
(K) Motif enrichment for Scute and Asense transcription factors in less accessible peaks upon *H1* knockdown.

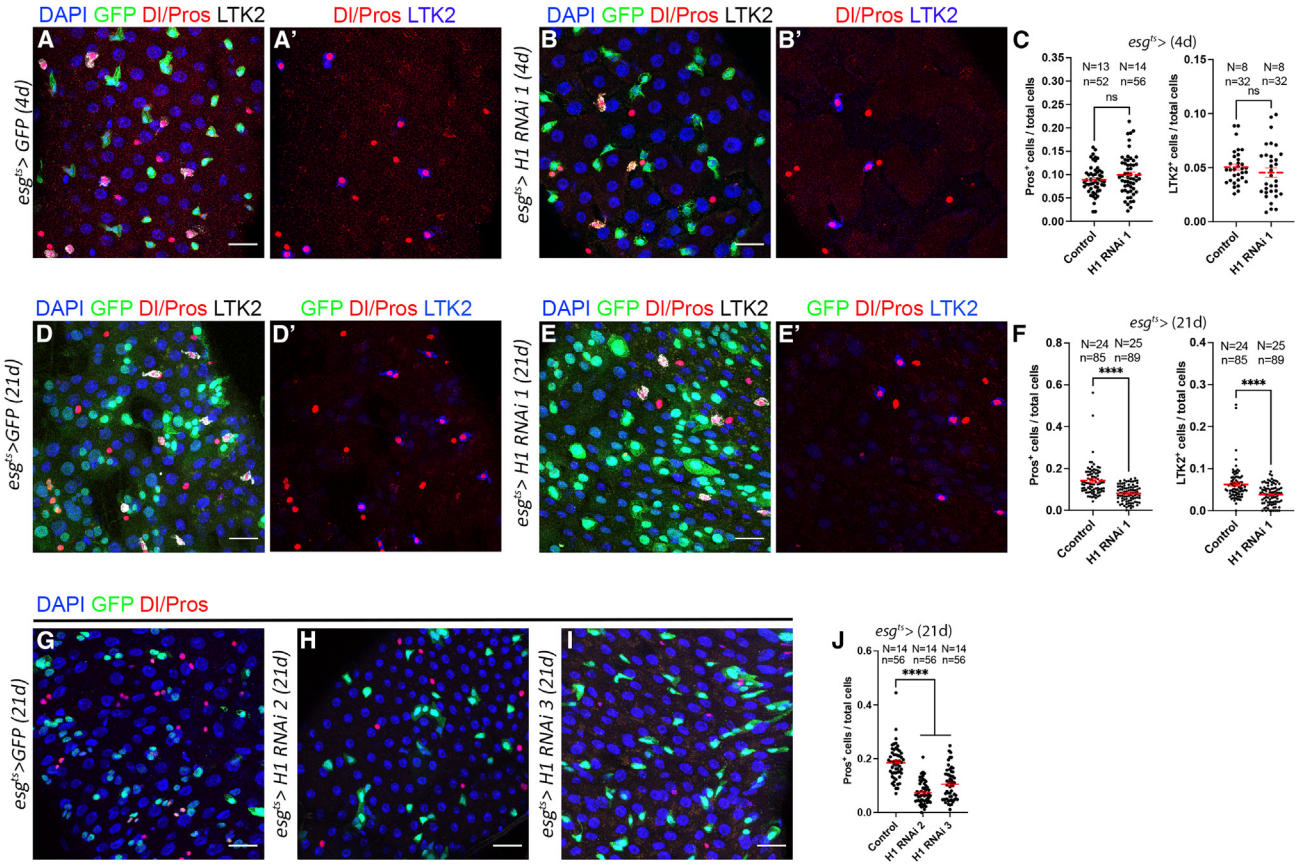

Figure 7. *H1* is required for ISC-lineage priming toward the EE fate

(A–B′) Representative images of control midgut (A and A′) and midgut after 4 days expression of *H1* RNAi 1 (B and B′) in ISCs/EBs (*esg*^{ts}) marked by GFP and stained for ISC marker (Delta) and EE markers LTK2 (type II EEs) and Pros (all EEs).

(C) Quantification of the ratios of Pros^{+} cells and LTK2^{+} cells per total cells in each image from (A)–(B′).

(D–E′) Representative images of control midgut (D and D′) and midgut after 21 days expression of *H1* RNAi 1 (E and E′) in ISCs/EBs (*esg*^{ts}) marked by GFP and stained for LTK2, Delta, and Pros.

(F) Ratios of Pros^{+} cells and LTK2^{+} cells per total cells in each image from (D)–(E′).

(G–I) Representative images of control midgut (G) and midgut after 21 days expression of *H1* RNAi 2 (H) or *H1* RNAi 3 (I) in ISCs and EBs (*esg*^{ts}).

(J) Quantification of the ratio of Pros^{+} cells per total cells in each image from (G)–(I). Scale bars, 20 μm. Two-tailed Mann-Whitney test. Mean values in red, error bars are SEM. ns for non-significant, ****$p < 0.0001$. N = number of guts, n = number of cells.

genes, or that H1 could maintain global compaction, limiting the access to transcriptional repressors specifically targeting EE genes. Consistent with this notion, we found that upon *H1* knockdown, there was a decrease in accessibility of peaks having motifs for the TFs, Sc, and Ase, which we previously demonstrated to be essential for EE fate specification.[78] Why EC-identity genes are not similarly primed by H1 is currently unclear. Therefore, this study identifies a role for H1 in regulating cell-fate decisions in an adult tissue. Interestingly, it was shown in the *Drosophila* adult ovary that H1 maintains germline stem cells, likely by preventing premature differentiation,[42] implying that H1 may have additional roles in other adult stem cell lineages.

Overall, our characterization of chromatin state transitions in the *Drosophila* intestinal lineage *in vivo* unveils insight into the modes of regulation of genes critical for stem cell activity and differentiation, as well as physiology-related genes specific of midgut terminally differentiated cells. Our data provide a large resource for investigating further aspects of chromatin regulation in this adult homeostatic tissue, as well as in other contexts such as environmental stress and disease.

Limitations of the study

DamID spatial resolution is limited by the distribution of GATC sites in the genome. However, comparison with ChIP-seq data previously showed that DamID is robust, reproducible, and sensitive.[79] To avoid non-specific methylation, the time of expression of Dam-fusion proteins is kept short (1 day) and at low levels using a bicistronic construct with the Dam-fusion sequence positioned downstream of another open reading frame coding for the Cherry fluorescent protein.[43]

The chromatin state models described here were verified through a number of independent methods, including the use of Akaike information criterion (AIC) to determine the optimum number of states, and PCA of state emissions to validate state clustering. However, as with all model inferences from genome-wide binding data, we cannot exclude the possibility that

chromatin state assignment does not fully explain the biology of a particular genomic locus. Although our findings bring insights into the biology of adult tissue differentiation on a systems level, we encourage the community to verify protein binding and chromatin state assignments in a genome browser before making interpretations regarding particular genes, to fully exploit this large resource.

STAR★METHODS

Detailed methods are provided in the online version of this paper and include the following:

- KEY RESOURCES TABLE
- RESOURCE AVAILABILITY
  - Lead contact
  - Materials availability
  - Data and code availability
- EXPERIMENTAL MODEL AND STUDY PARTICIPANT DETAILS
  - Fly stocks
- METHOD DETAILS
  - Targeted DamID
  - RNA-seq
  - ATAC-seq
  - GAL4 and clonal expression of H1 RNAi
  - Immunostaining
  - Imaging and quantifications
- QUANTIFICATION AND STATISTICAL ANALYSIS

SUPPLEMENTAL INFORMATION

Supplemental information can be found online at https://doi.org/10.1016/j.devcel.2023.11.005.

ACKNOWLEDGMENTS

We thank members of the Bardin team, M. van den Beek, C. Maurange, P.-A. Defossez, M. Wassef, and D. Bourc'his for comments on the manuscript. We thank A. Brand, A.I. Skoultchi, Bloomington, Vienna, and NIG, Kyoto stock centers for fly lines, and J. Veenstra for the LTK2 antibody. We thank S. Baulande and V. Raynal for help with high-throughput sequencing performed by the ICGex NGS platform of the Institut Curie, supported by the grants ANR-10-EQPX-03 (Equipex) and ANR-10-INBS-09-08 (France Génomique Consortium) from the Agence Nationale de la Recherche ("Investissements d'Avenir" program), by the Canceropole Ile-de-France, and by the SiRIC-Curie program—SiRIC Grant "INCa-DGOS4654." Microscopy training and access has been provided by The Cell and Tissue Imaging Facility/UMR3215 (PICT-IBiSA) of the Institut Curie, members of the French National Research Infrastructure France-BioImaging, ANR10-INBS-04. O.J.M. was supported by NHMRC grants APP1185220 and APP1128784. Work in the Bardin lab is supported by Fondation pour la Recherche Médicale (A.J.B., EQ202003010251), Fondation ARC (L.G., PJA20191209548), the program "Investissements d'Avenir" launched by the French Government and implemented by ANR, ANR SoMuSeq-STEM (A.J.B., ANR-16-CE13-0012-01), ANR ChronoDamage (A.J.B., ANR-20-CE13-0013_01), Labex DEEP (ANR11-LBX-0044), and IDEX PSL (ANR-10-IDEX-0001-02 PSL). Salary support for M.J. was from Ministère de l'Enseignement Supérieur (doctoral grant) and Fondation pour la Recherche Médicale (FDT202106012783); for A.J.B. and L.G. salary support was from the CNRS.

AUTHOR CONTRIBUTIONS

M.J., L.G., and A.J.B. designed the study. N.R. performed the chromatin state modeling, supervised by N.S. using the software and advice of O.J.M. M.J., L.G., O.J.M., N.R., and A.J.B. analyzed the data. M.J., L.G., and S.R. performed genetic experiments. M.J. performed DamID, RNA-seq experiments, and analyses. L.G. performed ATAC-seq experiments and analyses. M.S. helped with RNA-seq and ATAC-seq experiments. M.E. optimized RNA-seq protocols. L.G. and A.J.B. supervised the study. M.J., O.J.M., L.G., and A.J.B. wrote the manuscript.

DECLARATION OF INTERESTS

The authors declare no competing interests.

Received: February 6, 2023
Revised: July 20, 2023
Accepted: November 10, 2023
Published: December 5, 2023

REFERENCES

1. Flavahan, W.A., Gaskell, E., and Bernstein, B.E. (2017). Epigenetic plasticity and the hallmarks of cancer. Science *357*.
2. Avgustinova, A., and Benitah, S.A. (2016). Epigenetic control of adult stem cell function. Nat. Rev. Mol. Cell Biol. *17*, 643–658.
3. Atlasi, Y., and Stunnenberg, H.G. (2017). The interplay of epigenetic marks during stem cell differentiation and development. Nat. Rev. Genet. *18*, 643–658.
4. Argelaguet, R., Clark, S.J., Mohammed, H., Stapel, L.C., Krueger, C., Kapourani, C.-A., Imaz-Rosshandler, I., Lohoff, T., Xiang, Y., Hanna, C.W., et al. (2019). Multi-omics profiling of mouse gastrulation at single-cell resolution. Nature *576*, 487–491.
5. Mikkelsen, T.S., Ku, M., Jaffe, D.B., Issac, B., Lieberman, E., Giannoukos, G., Alvarez, P., Brockman, W., Kim, T.-K., Koche, R.P., et al. (2007). Genome-wide maps of chromatin state in pluripotent and lineage-committed cells. Nature *448*, 553–560.
6. Wu, J., Huang, B., Chen, H., Yin, Q., Liu, Y., Xiang, Y., Zhang, B., Liu, B., Wang, Q., Xia, W., et al. (2016). The landscape of accessible chromatin in mammalian preimplantation embryos. Nature *534*, 652–657.
7. Ernst, J., and Kellis, M. (2010). Discovery and characterization of chromatin states for systematic annotation of the human genome. Nat. Biotechnol. *28*, 817–825.
8. Filion, G.J., van Bemmel, J.G., Braunschweig, U., Talhout, W., Kind, J., Ward, L.D., Brugman, W., de Castro, I.J., Kerkhoven, R.M., Bussemaker, H.J., et al. (2010). Systematic protein location mapping reveals five principal chromatin types in drosophila cells. Cell *143*, 212–224.
9. Ho, J.W.K., Jung, Y.L., Liu, T., Alver, B.H., Lee, S., Ikegami, K., Sohn, K.-A., Minoda, A., Tolstorukov, M.Y., Appert, A., et al. (2014). Comparative analysis of metazoan chromatin organization. Nature *512*, 449–452.
10. Kharchenko, P.V., Alekseyenko, A.A., Schwartz, Y.B., Minoda, A., Riddle, N.C., Ernst, J., Sabo, P.J., Larschan, E., Gorchakov, A.A., Gu, T., et al. (2011). Comprehensive analysis of the chromatin landscape in *Drosophila melanogaster*. Nature *471*, 480–485.
11. Marshall, O.J., and Brand, A.H. (2017). Chromatin state changes during neural development revealed by in vivo cell-type specific profiling. Nat. Commun. *8*, 2271.
12. Gorkin, D.U., Barozzi, I., Zhao, Y., Zhang, Y., Huang, H., Lee, A.Y., Li, B., Chiou, J., Wildberg, A., Ding, B., et al. (2020). An atlas of dynamic chromatin landscapes in mouse fetal development. Nature *583*, 744–751.
13. Nègre, N., Brown, C.D., Ma, L., Bristow, C.A., Miller, S.W., Wagner, U., Kheradpour, P., Eaton, M.L., Loriaux, P., Sealfon, R., et al. (2011). A cis-regulatory map of the Drosophila genome. Nature *471*, 527–531.

14. van der Velde, A., Fan, K., Tsuji, J., Moore, J.E., Purcaro, M.J., Pratt, H.E., and Weng, Z. (2021). Annotation of chromatin states in 66 complete mouse epigenomes during development. Commun. Biol. *4*, 239.
15. Adam, R.C., Yang, H., Rockowitz, S., Larsen, S.B., Nikolova, M., Oristian, D.S., Polak, L., Kadaja, M., Asare, A., Zheng, D., et al. (2015). Pioneer factors govern super-enhancer dynamics in stem cell plasticity and lineage choice. Nature *521*, 366–370.
16. Jadhav, U., Nalapareddy, K., Saxena, M., O'Neill, N.K., Pinello, L., Yuan, G.-C., Orkin, S.H., and Shivdasani, R.A. (2016). Acquired tissue-specific promoter bivalency is a basis for PRC2 necessity in adult cells. Cell *165*, 1389–1400.
17. Kazakevych, J., Sayols, S., Messner, B., Krienke, C., and Soshnikova, N. (2017). Dynamic changes in chromatin states during specification and differentiation of adult intestinal stem cells. Nucleic Acids Res. *45*, 5770–5784.
18. Lien, W.-H., Guo, X., Polak, L., Lawton, L.N., Young, R.A., Zheng, D., and Fuchs, E. (2011). Genome-wide maps of histone modifications unwind in vivo chromatin states of the hair follicle lineage. Cell Stem Cell *9*, 219–232.
19. Raab, J.R., Tulasi, D.Y., Wager, K.E., Morowitz, J.M., Magness, S.T., and Gracz, A.D. (2020). Quantitative classification of chromatin dynamics reveals regulators of intestinal stem cell differentiation. Development *147*, 181966.
20. Lara-Astiaso, D., Weiner, A., Lorenzo-Vivas, E., Zaretsky, I., Jaitin, D.A., David, E., Keren-Shaul, H., Mildner, A., Winter, D., Jung, S., et al. (2014). Immunogenetics. Chromatin state dynamics during blood formation. Science *345*, 943–949.
21. Javierre, B.M., Burren, O.S., Wilder, S.P., Kreuzhuber, R., Hill, S.M., Sewitz, S., Cairns, J., Wingett, S.W., Várnai, C., Thiecke, M.J., et al. (2016). Lineage-specific genome architecture links enhancers and non-coding disease variants to target gene promoters. Cell *167*, 1369–1384.e19.
22. Gervais, L., and Bardin, A.J. (2017). Tissue homeostasis and aging: new insight from the fly intestine. Curr. Opin. Cell Biol. *48*, 97–105.
23. Jiang, H., Tian, A., and Jiang, J. (2016). Intestinal stem cell response to injury: lessons from Drosophila. Cell. Mol. Life Sci. *73*, 3337–3349.
24. Micchelli, C.A., and Perrimon, N. (2006). Evidence that stem cells reside in the adult Drosophila midgut epithelium. Nature *439*, 475–479.
25. Ohlstein, B., and Spradling, A. (2006). The adult Drosophila posterior midgut is maintained by pluripotent stem cells. Nature *439*, 470–474.
26. Chen, J., Xu, N., Wang, C., Huang, P., Huang, H., Jin, Z., Yu, Z., Cai, T., Jiao, R., and Xi, R. (2018). Transient scute activation via a self-stimulatory loop directs enteroendocrine cell pair specification from self-renewing intestinal stem cells. Nat. Cell Biol. *20*, 152–161.
27. Boumard, B., and Bardin, A.J. (2021). An amuse-bouche of stem cell regulation: underlying principles and mechanisms from adult Drosophila intestinal stem cells. Curr. Opin. Cell Biol. *73*, 58–68.
28. Amcheslavsky, A., Nie, Y., Li, Q., He, F., Tsuda, L., Markstein, M., and Ip, Y.T. (2014). Gene expression profiling identifies the zinc-finger protein Charlatan as a regulator of intestinal stem cells in Drosophila. Development *141*, 2621–2632.
29. Andriatsilavo, M., Stefanutti, M., Siudeja, K., Perdigoto, C.N., Boumard, B., Gervais, L., Gillet-Markowska, A., Al Zouabi, L., Schweisguth, F., and Bardin, A.J. (2018). Spen limits intestinal stem cell self-renewal. PLoS Genet. *14*, e1007773.
30. Buszczak, M., Paterno, S., and Spradling, A.C. (2009). Drosophila stem cells share a common requirement for the histone H2B ubiquitin protease scrawny. Science *323*, 248–251.
31. Brodsly, N.F., Bitman-Lotan, E., Boico, O., Shafat, A., Monastirioti, M., Gessler, M., Delidakis, C., Rincon-Arano, H., and Orian, A. (2019). The transcription factor Hey and nuclear lamins specify and maintain cell identity. eLife *8*, e44745.
32. Gervais, L., van den Beek, M., Josserand, M., Sallé, J., Stefanutti, M., Perdigoto, C.N., Skorski, P., Mazouni, K., Marshall, O.J., Brand, A.H., et al. (2019). Stem cell proliferation is kept in check by the chromatin regulators kismet/CHD7/CHD8 and Trr/MLL3/4. Dev. Cell *49*, 556–573.e6.
33. Jin, Y., Xu, J., Yin, M.X., Lu, Y., Hu, L., Li, P., Zhang, P., Yuan, Z., Ho, M.S., Ji, H., et al. (2013). Brahma is essential for Drosophila intestinal stem cell proliferation and regulated by Hippo signaling. eLife *2*, e00999.
34. Ma, Y., Chen, Z., Jin, Y., and Liu, W. (2013). Identification of a histone acetyltransferase as a novel regulator of *Drosophila* intestinal stem cells. FEBS Lett. *587*, 1489–1495.
35. Tauc, H.M., Rodriguez-Fernandez, I.A., Hackney, J.A., Pawlak, M., Ronnen Oron, T., Korzelius, J., Moussa, H.F., Chaudhuri, S., Modrusan, Z., Edgar, B.A., et al. (2021). Age-related changes in polycomb gene regulation disrupt lineage fidelity in intestinal stem cells. eLife *10*, e62250.
36. Tauc, H.M., Tasdogan, A., Meyer, P., and Pandur, P. (2017). Nipped-A regulates intestinal stem cell proliferation in Drosophila. Development *144*, 612–623.
37. Zeng, X., Lin, X., and Hou, S.X. (2013). The Osa-containing SWI/SNF chromatin-remodeling complex regulates stem cell commitment in the adult Drosophila intestine. Development *140*, 3532–3540.
38. Prendergast, L., and Reinberg, D. (2021). The missing linker: emerging trends for H1 variant-specific functions. Genes Dev. *35*, 40–58.
39. Fyodorov, D.V., Zhou, B.-R., Skoultchi, A.I., and Bai, Y. (2018). Emerging roles of linker histones in regulating chromatin structure and function. Nat. Rev. Mol. Cell Biol. *19*, 192–206.
40. Bayona-Feliu, A., Casas-Lamesa, A., Carbonell, A., Climent-Cantó, P., Tatarski, M., Pérez-Montero, S., Azorín, F., and Bernués, J. (2016). Histone H1: lessons from drosophila. Biochim. Biophys. Acta *1859*, 526–532.
41. Pérez-Montero, S., Carbonell, A., Morán, T., Vaquero, A., and Azorín, F. (2013). The embryonic linker histone H1 variant of drosophila, dBigH1, regulates zygotic genome activation. Dev. Cell *26*, 578–590.
42. Sun, J., Wei, H.-M., Xu, J., Chang, J.-F., Yang, Z., Ren, X., Lv, W.-W., Liu, L.-P., Pan, L.-X., Wang, X., et al. (2015). Histone H1-mediated epigenetic regulation controls germline stem cell self-renewal by modulating H4K16 acetylation. Nat. Commun. *6*, 8856.
43. Southall, T.D., Gold, K.S., Egger, B., Davidson, C.M., Caygill, E.E., Marshall, O.J., and Brand, A.H. (2013). Cell-type-specific profiling of gene expression and chromatin binding without cell isolation: assaying RNA Pol II occupancy in neural stem cells. Dev. Cell *26*, 101–112.
44. Marshall, O.J., Southall, T.D., Cheetham, S.W., and Brand, A.H. (2016). Cell-type-specific profiling of protein–DNA interactions without cell isolation using targeted DamID with next-generation sequencing. Nat. Protoc. *11*, 1586–1598.
45. van Steensel, B., and Henikoff, S. (2000). Identification of in vivo DNA targets of chromatin proteins using tethered Dam methyltransferase. Nat. Biotechnol. *18*, 424–428.
46. Delandre, C., McMullen, J.P.D., Paulsen, J., Collas, P., and Marshall, O.J. (2022). Eight principal chromatin states functionally segregate the fly genome into developmental and housekeeping roles. Preprint at bioRxiv. https://doi.org/10.1101/2022.10.30.514435.
47. Aughey, G.N., Estacio Gomez, A., Thomson, J., Yin, H., and Southall, T.D. (2018). CATaDa reveals global remodelling of chromatin accessibility during stem cell differentiation in vivo. eLife *7*, e32341.
48. Dutta, D., Dobson, A.J., Houtz, P.L., Gläßer, C., Revah, J., Korzelius, J., Patel, P.H., Edgar, B.A., and Buchon, N. (2015). Regional cell-specific transcriptome mapping reveals regulatory complexity in the adult drosophila midgut. Cell Rep. *12*, 346–358.
49. Hawkins, R.D., Hon, G.C., Lee, L.K., Ngo, Q., Lister, R., Pelizzola, M., Edsall, L.E., Kuan, S., Luu, Y., Klugman, S., et al. (2010). Distinct epigenomic landscapes of pluripotent and lineage-committed human cells. Cell Stem Cell *6*, 479–491.
50. Delandre, C., and Marshall, O.J. (2019). United colours of chromatin? Developmental genome organisation in flies. Biochem. Soc. Trans. *47*, 691–700.

51. Wen, B., Wu, H., Shinkai, Y., Irizarry, R.A., and Feinberg, A.P. (2009). Large histone H3 lysine 9 dimethylated chromatin blocks distinguish differentiated from embryonic stem cells. Nat. Genet. *41*, 246–250.

52. Nicetto, D., and Zaret, K.S. (2019). Role of H3K9me3 heterochromatin in cell identity establishment and maintenance. Curr. Opin. Genet. Dev. *55*, 1–10.

53. Wang, C., Liu, X., Gao, Y., Yang, L., Li, C., Liu, W., Chen, C., Kou, X., Zhao, Y., Chen, J., et al. (2018). Reprogramming of H3K9me3-dependent heterochromatin during mammalian embryo development. Nat. Cell Biol. *20*, 620–631.

54. Hu, Y., Comjean, A., Perkins, L.A., Perrimon, N., and Mohr, S.E. (2015). GLAD: an Online Database of G ene L ist A nnotation for *D rosophila*. J. Genomics *3*, 75–81.

55. Lemaitre, B., and Miguel-Aliaga, I. (2013). The digestive tract of *Drosophila melanogaster*. Annu. Rev. Genet. *47*, 377–404.

56. Lu, X., Wontakal, S.N., Emelyanov, A.V., Morcillo, P., Konev, A.Y., Fyodorov, D.V., and Skoultchi, A.I. (2009). Linker histone H1 is essential for Drosophila development, the establishment of pericentric heterochromatin, and a normal polytene chromosome structure. Genes Dev. *23*, 452–465.

57. Lu, X., Wontakal, S.N., Kavi, H., Kim, B.J., Guzzardo, P.M., Emelyanov, A.V., Xu, N., Hannon, G.J., Zavadil, J., Fyodorov, D.V., et al. (2013). Drosophila H1 regulates the genetic activity of heterochromatin by recruitment of Su(var)3-9. Science *340*, 78–81.

58. Hu, J., Gu, L., Ye, Y., Zheng, M., Xu, Z., Lin, J., Du, Y., Tian, M., Luo, L., Wang, B., et al. (2018). Dynamic placement of the linker histone H1 associated with nucleosome arrangement and gene transcription in early Drosophila embryonic development. Cell Death Dis. *9*, 765.

59. Willcockson, M.A., Healton, S.E., Weiss, C.N., Bartholdy, B.A., Botbol, Y., Mishra, L.N., Sidhwani, D.S., Wilson, T.J., Pinto, H.B., Maron, M.I., et al. (2020). histones control the epigenetic landscape by local chromatin compaction. Nature *1–6*, 293–298.

60. Kim, T.-H., Li, F., Ferreiro-Neira, I., Ho, L.-L., Luyten, A., Nalapareddy, K., Long, H., Verzi, M., and Shivdasani, R.A. (2014). Broadly permissive intestinal chromatin underlies lateral inhibition and cell plasticity. Nature *506*, 511–515.

61. Loh, C.H., and Veenstra, G.J.C. (2022). The role of polycomb proteins in cell lineage commitment and embryonic development. Epigenomes *6*, 23.

62. Chen, X., Hiller, M., Sancak, Y., and Fuller, M.T. (2005). Tissue-specific TAFs counteract polycomb to turn on terminal differentiation. Science *310*, 869–872.

63. Li, X., Han, Y., and Xi, R. (2010). Polycomb group genes *Psc* and *Su(z)2* restrict follicle stem cell self-renewal and extrusion by controlling canonical and noncanonical Wnt signaling. Genes Dev. *24*, 933–946.

64. Li, X., Yang, F., Chen, H., Deng, B., Li, X., and Xi, R. (2016). Control of germline stem cell differentiation by polycomb and trithorax group genes in the niche microenvironment. Development *143*, 3449–3458.

65. Morillo Prado, J.R., Chen, X., and Fuller, M.T. (2012). Polycomb group genes Psc and Su(z)2 maintain somatic stem cell identity and activity in drosophila. PLoS One *7*, e52892.

66. Zhang, S., Pan, C., Lv, X., Wu, W., Chen, H., Wu, W., Wu, H., Zhang, L., and Zhao, Y. (2017). Repression of Abd-B by Polycomb is critical for cell identity maintenance in adult Drosophila testis. Sci. Rep. *7*, 5101.

67. Eun, S.H., Shi, Z., Cui, K., Zhao, K., and Chen, X. (2014). A non–cell autonomous role of E (z) to prevent germ cells from turning on a somatic cell marker. Science *343*, 1513–1516.

68. DeLuca, S.Z., Ghildiyal, M., Pang, L.-Y., and Spradling, A.C. (2020). Differentiating Drosophila female germ cells initiate Polycomb silencing by regulating PRC2-interacting proteins. eLife *9*, e56922.

69. Flora, P., Dalal, G., Cohen, I., and Ezhkova, E. (2021). Polycomb repressive complex(es) and their role in adult stem cells. Genes *12*, 1485.

70. Flora, P., Li, M.-Y., Galbo, P.M., Astorkia, M., Zheng, D., and Ezhkova, E. (2021). Polycomb repressive complex 2 in adult hair follicle stem cells is dispensable for hair regeneration. PLoS Genet. *17*, e1009948.

71. Nalabothula, N., McVicker, G., Maiorano, J., Martin, R., Pritchard, J.K., and Fondufe-Mittendorf, Y.N. (2014). The chromatin architectural proteins HMGD1 and H1 bind reciprocally and have opposite effects on chromatin structure and gene regulation. BMC Genomics *15*, 92.

72. Misteli, T., Gunjan, A., Hock, R., Bustin, M., and Brown, D.T. (2000). Dynamic binding of histone H1 to chromatin in living cells. Nature *408*, 877–881.

73. Lever, M.A., Th'ng, J.P., Sun, X., and Hendzel, M.J. (2000). Rapid exchange of histone H1.1 on chromatin in living human cells. Nature *408*, 873–876.

74. Fan, Y., Nikitina, T., Zhao, J., Fleury, T.J., Bhattacharyya, R., Bouhassira, E.E., Stein, A., Woodcock, C.L., and Skoultchi, A.I. (2005). Histone H1 depletion in mammals alters global chromatin structure but causes specific changes in gene regulation. Cell *123*, 1199–1212.

75. Torres, C.M., Biran, A., Burney, M.J., Patel, H., Henser-Brownhill, T., Cohen, A.-H.S., Li, Y., Ben-Hamo, R., Nye, E., Spencer-Dene, B., et al. (2016). The linker histone H1.0 generates epigenetic and functional intratumor heterogeneity. Science *353*, aaf1644.

76. Yusufova, N., Kloetgen, A., Teater, M., Osunsade, A., Camarillo, J.M., Chin, C.R., Doane, A.S., Venters, B.J., Portillo-Ledesma, S., Conway, J., et al. (2021). Histone H1 loss drives lymphoma by disrupting 3D chromatin architecture. Nature *589*, 299–305.

77. Serna-Pujol, N., Salinas-Pena, M., Mugianesi, F., Le Dily, F., Marti-Renom, M.A., and Jordan, A. (2022). Coordinated changes in gene expression, H1 variant distribution and genome 3D conformation in response to H1 depletion. Nucleic Acids Res. *50*, 3892–3910.

78. Bardin, A.J., Perdigoto, C.N., Southall, T.D., Brand, A.H., and Schweisguth, F. (2010). Transcriptional control of stem cell maintenance in the Drosophila intestine. Development *137*, 705–714.

79. Aughey, G.N., Cheetham, S.W., and Southall, T.D. (2019). DamID as a versatile tool for understanding gene regulation. Development *146*, dev173666.

80. Furriols, M., and Bray, S. (2001). A model Notch response element detects Suppressor of Hairless–dependent molecular switch. Curr. Biol. *11*, 60–64.

81. Zeng, X., Chauhan, C., and Hou, S.X. (2010). Characterization of midgut stem cell- and enteroblast-specific Gal4 lines in drosophila. Genesis *48*, 607–611.

82. Jiang, H., Patel, P.H., Kohlmaier, A., Grenley, M.O., McEwen, D.G., and Edgar, B.A. (2009). Cytokine/jak/stat signaling mediates regeneration and homeostasis in the drosophila midgut. Cell *137*, 1343–1355.

83. Wang, C., Guo, X., and Xi, R. (2014). EGFR and Notch signaling respectively regulate proliferative activity and multiple cell lineage differentiation of Drosophila gastric stem cells. Cell Res. *24*, 610–627.

84. Balakireva, M., Stocker, R.F., Gendre, N., and Ferveur, J.-F. (1998). Voila, a new drosophila courtship variant that affects the nervous system: behavioral, neural, and genetic characterization. J. Neurosci. *18*, 4335–4343.

85. Marshall, O.J., and Brand, A.H. (2015). damidseq_pipeline: an automated pipeline for processing DamID sequencing datasets. Bioinformatics *31*, 3371–3373.

86. Langmead, B., and Salzberg, S.L. (2012). Fast gapped-read alignment with Bowtie 2. Nat. Methods *9*, 357–359.

87. Quinlan, A.R., and Hall, I.M. (2010). BEDTools: a flexible suite of utilities for comparing genomic features. Bioinformatics *26*, 841–842.

88. Love, M.I., Huber, W., and Anders, S. (2014). Moderated estimation of fold change and dispersion for RNA-seq data with DESeq2. Genome Biol. *15*, 550.

89. Ramírez, F., Ryan, D.P., Grüning, B., Bhardwaj, V., Kilpert, F., Richter, A.S., Heyne, S., Dündar, F., and Manke, T. (2016). deepTools2: a next

generation web server for deep-sequencing data analysis. Nucleic Acids Res. *44*, W160–W165.

90. Zhang, Y., Liu, T., Meyer, C.A., Eeckhoute, J., Johnson, D.S., Bernstein, B.E., Nusbaum, C., Myers, R.M., Brown, M., Li, W., et al. (2008). Model-based analysis of ChIP-seq (MACS). Genome Biol. *9*, R137.
91. Ross-Innes, C.S., Stark, R., Teschendorff, A.E., Holmes, K.A., Ali, H.R., Dunning, M.J., Brown, G.D., Gojis, O., Ellis, I.O., Green, A.R., et al. (2012). Differential oestrogen receptor binding is associated with clinical outcome in breast cancer. Nature *481*, 389–393.
92. Yu, G., Wang, L.-G., and He, Q.-Y. (2015). ChIPseeker: an R/Bioconductor package for ChIP peak annotation, comparison and visualization. Bioinformatics *31*, 2382–2383.
93. Bailey, T.L., Johnson, J., Grant, C.E., and Noble, W.S. (2015). The MEME suite. Nucleic Acids Res. *43*, W39–W49.
94. Afgan, E., Baker, D., van den Beek, M., Blankenberg, D., Bouvier, D., Čech, M., Chilton, J., Clements, D., Coraor, N., Eberhard, C., et al. (2016). The Galaxy platform for accessible, reproducible and collaborative biomedical analyses: 2016 update. Nucleic Acids Res. *44*, W3–W10.
95. Gu, Z., Eils, R., and Schlesner, M. (2016). Complex heatmaps reveal patterns and correlations in multidimensional genomic data. Bioinformatics *32*, 2847–2849.
96. Gel, B., and Serra, E. (2017). karyoploteR: an R/Bioconductor package to plot customizable genomes displaying arbitrary data. Bioinformatics *33*, 3088–3090.
97. Thomas, P.D., Ebert, D., Muruganujan, A., Mushayahama, T., Albou, L.P., and Mi, H. (2022). PANTHER: making genome-scale phylogenetics accessible to all. Protein Sci. *31*, 8–22.
98. Bankhead, P., Loughrey, M.B., Fernández, J.A., Dombrowski, Y., McArt, D.G., Dunne, P.D., McQuaid, S., Gray, R.T., Murray, L.J., Coleman, H.G., et al. (2017). QuPath: open source software for digital pathology image analysis. Sci. Rep. *7*, 16878.
99. Robinson, J.T., Thorvaldsdóttir, H., Winckler, W., Guttman, M., Lander, E.S., Getz, G., and Mesirov, J.P. (2011). Integrative genomics viewer. Nat. Biotechnol. *29*, 24–26.
100. Guo, X., Yin, C., Yang, F., Zhang, Y., Huang, H., Wang, J., Deng, B., Cai, T., Rao, Y., and Xi, R. (2019). The cellular diversity and transcription factor code of drosophila enteroendocrine cells. Cell Rep. *29*, 4172–4185.e5.
101. Buenrostro, J.D., Wu, B., Chang, H.Y., and Greenleaf, W.J. (2015). ATAC-seq: A method for assaying chromatin accessibility genome-wide. Curr. Protoc. Mol. Biol. *109*, 21.29.1–21.29.9.

STAR★METHODS

KEY RESOURCES TABLE

REAGENT or RESOURCE	SOURCE	IDENTIFIER
Antibodies		
Mouse anti-Delta ECD (1:2000)	DSHB	Cat# c594.9b, RRID: AB_528194
Mouse anti-Prospero (1:2000)	DSHB	Cat# Prospero (MR1A) RRID: AB_528440
Chicken anti-GFP (1:1000)	Invitrogen	Cat# A10262 RRID: AB_2534023
Goat anti-ßGAL (1:500)	Biogenesis	Cat# 466-1409
Rabbit anti-PH3 (1:1000)	Millipore	Cat# 06-570 RRID:AB_310177
Rabbit anti-LTK2 (1:1000)	Gift from J.A Veenstra, Université de Bordeaux	Cat# Veenstra_001 RRID: AB_2923320
Moue anti-H1 (1:300)	Active motif	Cat# 61785 RRID: AB_2793765
Rabbit anti-DsRed (1:1000)	Takara Bio	Cat# 632496 RRID: AB_10013483
Chemicals, peptides, and recombinant proteins		
RNase A	Sigma	Cat# R6513-50MG
Quick ligase	New England Biolabs	Cat# M2200S
T4 DNA ligase	New England Biolabs	Cat# M0202S
T4 DNA Polymerase	New England Biolabs	Cat# M0203S
T4 polynucleotide kinase	New England Biolabs	Cat# M0201S
Klenow fragment	New England Biolabs	Cat# M0210S
CutSmart Buffer	New England Biolabs	Cat# B7204S
DpnI	New England Biolabs	Cat# R0176L
DpnII	New England Biolabs	Cat# R0543L
Sau3AI	New England Biolabs	Cat# R0169L
AlwI	New England Biolabs	Cat# R0513S
MyTaq HS DNA Polymerase	Bioline	Cat# BIO-21111
Elastase	Sigma	Cat# E0258-5MG
2x TD buffer	Illumina	Cat# FC-121-1030
Tn5 Transposase	Illumina	Cat# FC-121-1030
SYBR™ Green I Nucleic Acid	Thermo Fisher	Cat# S7563
Critical commercial assays		
QIAquick PCR Purification Kit	Qiagen	Cat# 28104
QIAmp DNA Micro Kit	Qiagen	Cat# 56304
NEBNext High-Fidelity 2X PCR Master Mix	New England Biolabs	Cat# M0541S
Seramag SpeedBeads	Fisher Scientific	Cat# 12326433
Qubit dsDNA HS Assay	ThermoFisher Scientific	Cat# Q32851
Bioanalyzer DNA analysis	Agilent	Cat# 5067
RNase-Free DNase Set	Qiagen	Cat# 79254
Arcturus PicoPure RNA Isolation Kit	ThermoFisher Scientific	Cat# KIT0204
Qubit RNA HS Assay	ThermoFisher Scientific	Cat# Q32852
Illumina Stranded mRNA Prep	Illumina	Cat# 20040534
Nextera DNA Library Prep Kit	Illumina	Cat# FC-121-1030
Qiagen MinElute Reaction Cleanup Kit	Qiagen	Cat# 28204
Agencourt AMPure XP beads	Fisher Scientific	Cat# 10136224

(*Continued on next page*)

Continued

REAGENT or RESOURCE	SOURCE	IDENTIFIER
IDT® for Illumina Nextera DNA Unique Dual Indexes	Illumina	Cat# 20026121
Deposited data		
Lists of expressed genes and cell type-specific genes generated from published RNAseq data in the gut	Dutta et al.[48]	http://flygutseq.buchonlab.com/resources
DamID data for RNA Pol II, Brm, Pc, H 1 and HP1 in ISC	Gervais et al.[32]	GEO: GSE128941
Raw and processed data (DamID, RNA-seq, ATAC-seq)	This paper	GEO: GSE224967
Chromatin state tracks per cell type	This paper	https://github.com/gervlouis/Josserand_et_al https://doi.org/10.5281/zenodo.10044614
Experimental models: Organisms/strains		
Drosophila: UAS-LT3-NDam	Southall et al.[43]	N/A
Drosophila: UAS-LT3-NDam-RPII215	Southall et al.[43]	N/A
Drosophila: UAS-LT3-Dam-Pc	Marshall and Brand[11]	N/A
Drosophila: UAS-LT3-Dam-HP1a	Marshall and Brand[11]	N/A
Drosophila: UAS-LT3-Dam-Brm	Marshall and Brand[11]	N/A
Drosophila: UAS-LT3-Dam-H 1	Marshall and Brand[11]	N/A
Drosophila: Su(H)GBE-LacZ	Furriols and Bray[80]	N/A
Drosophila: Su(H)GBE-GAL4; tubGAL80^{ts} UAS-GFP	Zeng et al.[81]	N/A
Drosophila: esg-GAL4, tubGAL80ts UAS-GFP	Jiang et al.[82]	N/A
Drosophila: esg-GAL4 UAS-YFP; Su(H)GBE-GAL80 tubGAL80^{ts}	Wang et al.[83]	N/A
Drosophila: MyoIAGAL4; tubGAL80^{ts} UAS-GFP	Jiang et al.[82]	N/A
Drosophila: pros^{voila}-GAL4, tub-GAL80ts	Balakireva et al.[84]	N/A
Drosophila: esgGAL4 UAS-GFP tubGAL80ts;UAS-FLP act-FRT-CD2-FRT-GAL4	Jiang et al.[82]	N/A
Drosophila: UAS-H1-RNAi pINT-1-H15M	Lu et al.[56]	N/A
UAS-H1-RNAi 1	NIG Fly stock center	Cat# 31617-R3
UAS-H1-RNAi 3	NIG Fly stock center	Cat# 31617-R2
Software and algorithms		
Prism 9	GraphPad Software	RRID:SCR_002798
Fiji	NIH	RRID:SCR_002285
RStudio	RStudio	RRID:SCR_000432
damidseq_pipeline	Marshall and Brand[85]	https://github.com/owenjm/damidseq_pipeline
bowtie2	Langmead and Salzberg[86]	http://bowtie-bio.sourceforge.net/bowtie2/index.shtml
bedtools	Quilan and Hall[87]	https://bedtools.readthedocs.io/en/latest/index.html
DESeq2	Love et al.[88]	https://bioconductor.org/packages/release/bioc/html/DESeq2.html
deepTools plotHeatmap	Ramírez et al.[89]	https://deeptools.readthedocs.io/en/develop/content/tools/plotHeatmap.html
MACS2	Zhang et al.[90]	https://github.com/taoliu/MACS
DiffBind	Ross-Innes et al.[91]	http://bioconductor.org/packages/release/bioc/html/DiffBind.html
ChIPseeker	Yu et al.[92]	http://bioconductor.org/packages/release/bioc/html/ChIPseeker.html

(*Continued on next page*)

Continued

REAGENT or RESOURCE	SOURCE	IDENTIFIER
MEME (5.4.1)	Bailey et al.[93]	http://meme-suite.org
polii.gene.call	Marshall and Brand[85]	https://github.com/owenjm/polii.gene.call
Galaxy	Afgan et al.[94]	https://usegalaxy.org
Peak_Calling_for_CATaDa	Aughey et al.[47]	https://github.com/tonysouthall/Peak_Calling_for_CATaDa
Universal Chromatin HMM script	Delandre et al.[46]	github.com/marshall-lab/universal_chromatin_hmm https://doi.org/10.5281/zenodo.10049873
ComplexHeatmap R package	Gu et al.[95]	https://github.com/jokergoo/ComplexHeatmap
karyoploteR	Gel et al.[96]	https://github.com/bernatgel/karyoploteR
SankeyMATIC	https://sankeymatic.com	https://github.com/nowthis/sankeymatic
PANTHER GO Enrichment Analysis	Thomas et al.[97]	http://geneontology.org/
bioinfo-pf-curie/RNA-seq: v4.0.0	Institut Curie	https://doi.org/10.5281/zenodo.7443721
bioinfo-pf-curie/ATAC-seq: v1.0.2 pipeline	Institut Curie	https://doi.org/10.5281/zenodo.7443721
QuPath	Bankhead et al.[98]	https://github.com/qupath/qupath/releases
IGV	Robinson et al.[99]	https://igv.org/

RESOURCE AVAILABILITY

Lead contact

Further information and requests for resources and reagents should be directed to and will be fulfilled by the lead contact, Allison Bardin (allison.bardin@curie.fr).

Materials availability

This study did not generate new unique reagents.

Data and code availability

- DamID data, RNA-seq data, and ATAC-seq data have been deposited at GEO and are publicly available, accession numbers are listed in the key resources table. Chromatin state tracks for each cell type are at https://github.com/gervlouis/Josserand_et_al and are publicly available. DamID data for RNA Pol II, Brm, Pc, H1 and HP1 in ISC were part of a previous study of ours[32] and have been deposited at GEO. This study analyzes other existing, publicly available data. These accession numbers for the datasets are listed in the key resources table. Microscopy data reported in this paper will be shared by the lead contact upon request.
- The code used in this study, derived from Delandre et al.[46] is at github.com/marshall-lab/universal_chromatin_hmm and is publicly available. DOIs are listed in the key resources table.
- Any additional information required to reanalyze the data reported in this paper is available from the lead contact upon request.

EXPERIMENTAL MODEL AND STUDY PARTICIPANT DETAILS

Fly stocks

The following fly stocks were used: *Su(H)GBE-LacZ*,[80] *esg-GAL4; tub-GAL80^{ts} UAS-GFP* ("*esg^{ts}*"),[82] *esg-GAL4 UAS-GFP; Su(H)GBE-GAL80 tub-GAL80^{ts}* ("*esg^{ts} Su(H)GBE-GAL80*"),[83] *Su(H)GBE-GAL4 UAS-GFP; tub-GAL80^{ts}* ("*Su(H)GBE^{ts}*"),[81] *MyoIA-GAL4; tub-GAL80^{ts} UAS-GFP* ("*Myo^{ts}*"),[82] *pros^{Voila}-GAL4 tub-GAL80^{ts}* ("*pros^{ts}*"),[84] *esg-GAL4 UAS-GFP tub-GAL80^{ts}; UAS-FLP act-FRT-CD2-FRT-GAL4* ("*esg-flpout*"),[82] *UAS-H 1-RNAi pINT-1-H 1^{5M}* ("*H 1-RNAi 2*" gift from A.I. Skoultchi),[56] 31617-R3 ("*H 1-RNAi 1*"), 31617-R2 ("*H 1-RNAi 3*") from the NIG Fly stock center (Kyoto), and *w^{1118}* (gift from M. McVey). For DamID experiments, fly lines were the following: *UAS-LT3-Ndam*, *UAS-LT3-Ndam-RpII215*, *UAS-LT3-Dam-Brm*, *UAS-LT3-Dam-Pc*, *UAS-LT3-Dam-HP1*, *UAS-LT3-Dam-H 1*.[11]

METHOD DETAILS

Targeted DamID

Library preparation

Expression of *UAS-Dam*, *UAS-Dam-RpII215*, *UAS-Dam-Brm*, *UAS-Dam-HP1*, *UAS-Dam-H1*, and *UAS-Dam-Pc* was targeted to specific cell types using GAL4 driver lines. ISC-specific expression was achieved with the *esg^{ts} Su(H)GBE-GAL80 driver*. *Su(H)GBE^{ts}* was used for EB-specific expression, *Myo^{ts}* for ECs and *pros^{ts}* for EEs. Crosses and their offspring were kept at 18°C to allow the

expression of the temperature sensitive Gal80^{ts} protein and therefore control temporally the expression of UAS-Dam constructs in ISCs. 2-3 day-old female flies with the correct genotype were shifted to 29°C (Gal80 restrictive temperature) for 1 day to induce Dam and Dam-fusion transgenes expression. For each experiment and replicate, 60 guts were dissected in PBS and immediately frozen in dry ice. Two or three biological replicates were performed for each experiment. Following tissue dissociation, genomic DNA was extracted from the guts and digested with DpnI to cut GATC methylated sites. DNA was purified and ligated with PCR adaptors specific to methylated fragments, before digestion with DpnII and PCR amplification. Then, DNA samples were purified and sonicated to reduce the fragment size to approximately 300 bp, followed by Alw1 digestion in order to remove DamID adaptors and initial GATC sequences. Digested DNA was purified with magnetic Seramag beads (FisherScientific) and end-repaired, adenylated, and ligated with Illumina TruSeq adaptors. Samples were subsequently cleaned twice with Seramag beads and enriched by 6 cycles of PCR, and cleaned again with Seramag beads.

Sequencing and data analysis

Samples were sequenced by a HiSeq 2500 (rapid run) to generate 50 bp single-end reads. The damidseq_pipeline script was used to align the NGS reads on the Drosophila reference genome and normalize them (log_2 ratio of Dam-fusion/Dam alone).[85] Correlations between the ratio files were calculated with the Pearson correlation coefficient. Replicates that correlated less than 0.8 with other replicates were discarded, leading to two or three replicates per experiment, that were averaged for further processing. Significant peaks were obtained by processing the ratio files with find_peaks (https://github.com/owenjm/find_peaks). All analyses were performed in the Galaxy server[94] and the visualization of alignments was performed using the IGV software.[99]

CATaDa analysis

Chromatin accessibility profiling was performed using Dam-only reference sequences generated for Targeted DamID (3 replicates per cell type). Fastq files were processed for CATaDa as previously described.[47] Reads were aligned to the *Drosophila melanogaster* reference genome version 6 and assigned to bins delimited by GATC sites using damidseq_pipeline_output_Dam-only_data. Peaks were called and mapped to genes, using Peak_Calling_for_CATaDa Perl program (FDR<0,01) and a consensus peak list was determined between each replicate. Scripts for CATaDa can be found at https://github.com/tonysouthall.

Chromatin state modeling

The log_2 ratio files obtained from damidseq_pipeline for the five proteins in bedgraph format were averaged and scaled by the standard deviation as previously described.[11] HMM modeling was performed using Universal Chromatin HMM script version 0.9.10 (github.com/marshall-lab/universal_chromatin_hmm) derived from ChroMATIC.[46] HMM models were trained on chromosomes 2L and 2R via 2000 random initializations of 10 iterations, followed by a full model fitted from the best-fitting random initialization parameters (as assessed via loglikelihood) and Viterbi paths determined, using the RHMM R package (https://r-forge.rproject.org/projects/rhmm/). Models with 5-40 states were fitted independently for each cell type, in order to allow the detection of chromatin state differences between cell types. HMM states were clustered based on their transition probabilities, and the clustering dendrogram was cut into 8 clusters. Each cluster was then assigned a chromatin state based on the strongest Pearson correlation between the mean state emissions of the cluster and the predefined intensities for 7 chromatin states (unpublished data provided by OJM). Finally, simplified Viterbi paths for the assigned chromatin states were created from this clustering. Manual adjustments to chromatin state calls were performed to correct some group misassignments. The optimum number of HMM states was determined via the Akaike information criterion (AIC) and manual inspection of the clustering dendrogram. Heatmaps of HMM state emissions were generated via the ComplexHeatmap R package.[95] Calculations of genome coverage and intersections with other datasets were performed using BEDtools in Galaxy (https://usegalaxy.eu/). The karyotype view in Figure S3C was generated using the R package karyoploteR (Rstudio version 2921.09.2).[96]

Gene chromatin state analysis

As per Marshall and Brand,[11] each gene was assigned a single chromatin state based on the prevalent state covering the gene length. Chromatin state transition plots were generated using SankeyMATIC (https://sankeymatic.com/). Cell-type specific RNA-seq data published in Dutta et al. can be found on (http://flygutseq.buchonlab.com/). On the graphs presented in Figure S3, null values of rpkm were excluded for easier visualization. The list of gene-encoding transcription factors comes from https://www.flyrnai.org/tools/glad/web/. The list of EE-enriched genes was obtained as follows: gene ontology analysis enrichment was performed on a list of 827 EE-enriched genes (from[48]), then only the genes associated with the enriched GO terms were kept (316 genes) and some-well known EE markers (from Guo et al.[100]) were manually added while TF-encoding genes were removed (final list of 321 genes). Gene Ontology enrichment analysis was carried out using http://geneontology.org/ [97] and redundant terms were manually removed. Graphs were generated using Prism 9 or R packages.

RNA-seq

RNA isolation

H1 RNAi expression was induced in ISC/EB using the driver *esg-GAL4; tub-GAL80^{ts} UAS-GFP* (*esg^{ts}*) that combines the UAS-GAL4 system with the temperature sensitive GAL80^{ts} protein that allows temporal control of transgene expression. 3-day old female flies with *esg^{ts}, UAS-GFP* (control) or *esg^{ts}, UAS-GFP UAS-H1 RNAi* 1 (31617-R3 from NIG Fly stock center) were kept at 18°C for 2 days and shifted to 29°C for 4 days on poor food to induce RNAi expression. For each replicate, 70 guts (control and H1 RNAi) were dissected in cold PBS, dissociated in elastase and FACS-sorted to isolate GFP$^+$ cells (ISCs and EBs). RNA isolation and purification was then performed with the Arcturus PicoPure RNA Isolation kit (ThermoFisher Scientific). RNA libraries were prepared with the Illumina Stranded mRNA Prep Ligation kit by the NGS facility of the Institut Curie.

Sequencing and data analysis

Sequencing was carried out on the NovaSeq 6000 instrument from Illumina based on a 2*100 cycle mode (paired-end reads, 100 bases) to obtain around 44 million clusters (88 million raw paired-end reads) per sample. The Nextflow pipeline for RNA-seq data processing developed by the Curie Bioinformatics Core facility was used (https://doi.org/10.5281/zenodo.7443721). FastQ files were generated with bcl2Fastq, demultiplexed and trimmed to remove adaptors using the Raw-QC and RNA-seq analysis pipelines. Reads were aligned to the *Drosophila* reference genome (dm6) to generate raw counts tables. Differential expression analysis was carried out with DESeq2[88] in Galaxy. Genes were filtered for p-adjusted value<0.05 to be considered as significantly deregulated genes. List of genes were further analyzed in Excel.

ATAC-seq

DNA tagmentation and isolation

3-day old female flies with *esg*^{ts}*, UAS-GFP* (control) or *esg*^{ts}*, UAS-GFP UAS-H1 RNAi 1* were kept at 18°C for 2 days and shifted to 29°C for 4 days on poor food to induce RNAi expression. ISCs and EBs were sorted by FACS. ATAC-seq protocol was adapted to the fly intestine from.[101] For each replicate, we collected a minimum of 50,000-100,000 GFP$^+$ progenitor cells. Sorted cells were washed in cold PBS and spun down at 4°C. The pellets were suspended in transposition mix (Illumina) and incubated at 37 °C for 30 min. The tagmented DNA was then purified using the Qiagen MinElute Cleanup Kit. Purified transposed samples were amplified by PCR using the NEBNext Hi-Fi 2X PCR Master Mix (New England Biolabs) and Illumina Nextera DNA Unique Dual Indexes. Determination of the cycle number at which each sample produced 25% of maximum fluorescent intensity was determined by qPCR. Amplified libraries were then purified using Qiagen MinElute Cleanup Kit and AMPure XP beads (Fisher Scientific) for double size selection. Library yield was assessed using the Qubit dsDNA HS assay kit (ThermoFisher Scientific) while library quality and molarity calculation were determined using Agilent Bioanalyzer high sensitivity DNA kits.

Sequencing and data analysis

Libraries were pooled and sequenced on the NovaSeq 6000 instrument from Illumina based on a 2*50 cycle mode (paired-end reads, 50 bases) using a SP flow cell in order to obtain around 67 million clusters (134 milion raw paired-end reads) per sample. Bioinfo-pf-curie/ATAC-seq: v1.0.2 pipeline for ATAC-seq data processing developed by the Curie Bioinformatics Core facility was used (https://doi.org/10.5281/zenodo.7576558). Raw reads were trimmed for adapters using trimgalore and aligned to the *Drosophila melanogaster* reference genome (dm6) using bowtie2.[86] Duplicated reads were removed from the aligned results with Picard, and filtered to discard low mapping quality reads <20, aligned to mitochondrial chromosome reads as well as singleton reads. Only valid pairs were considered. Read shifting was applied to account for Tn5 insertions (+ strand reads adjusted by 4 bp, and – strand reads adjusted by -5bp). Peaks were called using MACS[90] and Narrow peaks with q<0.01 were reported. Peak sets per conditions (control and H 1 RNAi) were obtained using bedtools Multiple Intersect between replicates.[87] Differential peaks analysis between conditions was performed with DiffBind[91] with significance set at FDR < 0.05. Peak Annotation was performed with ChIPseeker[92] with TSS region defined at -3kb to +3kb and all genes within the 10kb distance are reported for each peak. MEME (5.4.1)[93] was used to find enriched motifs in differentially accessible peaks. Metaplots were produced using deepTools plotHeatmap[89] in Galaxy.

GAL4 and clonal expression of H1 RNAi

H1 RNAi expression was induced in specific cell types using the UAS-GAL4 system combined with the temperature sensitive Gal80^{ts} protein that allows temporal control of transgene expression. The following drivers were used: for ISCs and EBs - "*esg*^{ts}"; for ISCs alone - "*esg*^{ts}*, Su(H)GBE-GAL80*"; for EBs - "*Su(H)GBE*^{ts}"; for EEs - "*pros*^{ts}"; for clonal expression - "*esg-flpout*". For quantification of the number of Pros$^+$ cells, Locustatachykinin$^+$ cells (LTK2), ßGAL$^+$ cells and the intensity of H 1 in GFP$^+$ cells, 3-day old female flies were shifted from 18°C to 29°C for 4 days (*esg*^{ts} experiments), 14 days (*esg-flpout* and *pros*^{ts} experiments) or 21 days (*esg*^{ts}, *Su(H)GBE*^{ts}, and *esg*^{ts} *Su(H)GBE-GAL80* experiments) to induce RNAi expression before dissection and immunostaining. All experiments have been done in 2 or 3 biological replicates with the exception of LTK2$^+$ cells quantification upon 4 days in *esg*^{ts}*>H1* knockdown and H1 level quantification upon 14 days in *pros*^{ts}*>H1* knockdown.

Immunostaining

Flies were dissected in PBS 1X to isolate whole guts associated with Malpighian tubules. Guts were fixated in 4% PFA for 2 h, rinsed in PBT (PBS 1X, 0,1% Triton-X 100) and then cut at the anterior and posterior sides in order to keep midguts only. Midguts were incubated in 50% glycerol/PBS 1X for 30 min to make waste exit by osmotic pressure upon rinsing with PBT, and incubated with primary antibodies overnight at 4°C. Then, midguts were rinsed with PBT and incubated with secondary antibodies for 3 h at room temperature. Next, they were washed in PBT and incubated with DAPI (1:1000,) for 5 min and equilibrated in 50% glycerol/PBS 1X before being mounted on slides in mounting medium.

The following primary antibodies were used: mouse anti-Delta (1:2000, DSHB C594.9B), chicken anti-GFP (1:1000, Invitrogen), mouse anti-Prospero (1:2000, DHSB), mouse anti-H1 (1:300, ActiveMotif), rabbit anti-LTK2 (1:1000, J.A. Veenstra), goat anti-ßGal (1:500, Biogenesis), rabbit anti-DsRed (1:1000, Takara).

Imaging and quantifications

Imaging was conducted using a Zeiss LSM900 confocal microscope and the ZEN software at the Curie Institute imaging facility (PICT). Images were acquired with a 40X oil objective. For stack images, z-step was set at 1 to 1.5 μm. For each midgut, four stacks

were taken corresponding to four different regions (R5, R4, R3, R2). Depending on the experiment, the number of GFP^+, $Pros^+$ cells, $LTK2^+$ cells, ECs, and total cells were quantified in each stack. Image analysis was performed using Fiji and QuPath[98] software followed by image assembly using Adobe Photoshop. Enterocytes (ECs) were identified and counted based on their nucleus size (nucleus diameter > 7μm). H1 and DAPI intensities in the nuclei of GFP^+ cells were quantified using QuPath. H1 intensity was then normalized to DAPI intensity.

QUANTIFICATION AND STATISTICAL ANALYSIS

All quantifications have been done both separately on biological replicates and on pooled replicates with the same results at the exception of the $Pros^+$ cells per total cells quantification after *H1* knockdown in EEs (Figure S7Q) for which two replicates and pooled data show no significant difference while one replicate shows a significant ($p<0.01$) decrease of the ratio. Statistical analyses were performed in Prism using the two-tailed Mann-Whitney test or Wilcoxon test. Significant values were reported as ns for non-significant, * for $p<0.05$, ** for $p<0.01$, *** for $p<0.001$ and **** for $p<0.0001$.